JPET Fast Forward. Published on November 7, 2016 as DOI: 10.1124/jpet.116.236224
This article has not been copyedited and formatted. The final version may differ from this version.

1. Title Page

BTK small molecule inhibitors induce a distinct pancreatic toxicity in rats[†]

Authors:

Rebecca I. Erickson*, Leah K. Schutt*, Jacqueline Tarrant, Michelle McDowell, Lichuan Liu, Adam R. Johnson, Sock-Cheng Lewin-Koh, Maj Hedehus, Jed Ross, Richard A. D. Carano, Karin Staflin, Fiona Zhong, James Crawford, Shelly Zhong, Karin Reif, Arna Katewa, Harvey Wong, Wendy Young, Donna Dambach, Dinah Misner

Author Affiliations:

Genentech, Inc. (RE, LS, JT, MM, LL, AJ, SL, MH, JR, RC, KS, FZ, JC, SZ, KR, WY, DD, DM) and University of British Columbia, Vancouver, B.C. (HW).

Primary Laboratory of Origin:

Genentech, Inc.

1 DNA Way, MS59

South San Francisco, CA, 94080

Downloaded from jpet.aspetjournals.org at ASPET Journals on April 18, 2024

JPET Fast Forward. Published on November 7, 2016 as DOI: 10.1124/jpet.116.236224
This article has not been copyedited and formatted. The final version may differ from this version.

2. Running Title Page

BTK inhibitors induce pancreatic toxicity in rats

Corresponding author:

Leah K. Schutt

1 DNA Way, MS59

South San Francisco, CA, 94080

Tel: 650-467-7712

Fax: 650-225-2797

schutt.leah@gene.com

Number of text pages: 38

Number of tables: 1

Number of figures: 8

Number of references: 39

Number of words in Abstract: 245

Number of words in Introduction: 750

Number of words in Discussion: 1406

List of nonstandard abbreviations: $AUC_{0\text{-}24}$, area under the concentration-time curve from time 0 to 24 hours; BCR, B-cell receptor; BTK, Bruton's tyrosine kinase; C_{max}, maximal concentration; CT, computed tomography; F-344; Fischer-344; IVGTT, intravenous

Downloaded from jpet.aspetjournals.org at ASPET Journals on April 18, 2024

JPET Fast Forward. Published on November 7, 2016 as DOI: 10.1124/jpet.116.236224
This article has not been copyedited and formatted. The final version may differ from this version.

glucose tolerance test; KO, knockout; LOAEL, low-observed-adverse-effect-level; MRI, magnetic resonance imaging; NOAEL, no-observed-adverse-effect-level; OGTT, oral glucose tolerance test; SD, Sprague-Dawley; T_{max}, time to maximal concentration; US, ultrasound; WH, Wistar-Han; XID, X-linked immunodeficient, XLA, X-linked agammaglobulinemia

Recommended section assignment: toxicology

Downloaded from jpet.aspetjournals.org at ASPET Journals on April 18, 2024

JPET Fast Forward. Published on November 7, 2016 as DOI: 10.1124/jpet.116.236224
This article has not been copyedited and formatted. The final version may differ from this version.

3. Abstract

Bruton's tyrosine kinase (BTK) is a member of the Tec family of cytoplasmic tyrosine kinases involved in B-cell and myeloid cell signaling. Small molecule inhibitors of BTK are being investigated for treatment of several hematological cancers and autoimmune diseases. GDC-0853 is a selective and reversible oral small molecule BTK inhibitor in development for the treatment of rheumatoid arthritis and systemic lupus erythematosus. In Sprague-Dawley (SD) rats, administration of GDC-0853 and other structurally diverse BTK inhibitors for 7 days or longer caused pancreatic lesions consisting of multifocal islet-centered hemorrhage, inflammation, fibrosis, and pigment-laden macrophages with adjacent lobular exocrine acinar cell atrophy, degeneration, and inflammation. Similar findings were not observed in mice or dogs at much higher exposures. Hemorrhage in the peri-islet vasculature emerged between 4 and 7 daily doses of GDC-0853 and was histologically similar to spontaneously occurring changes in aging SD rats. This suggests that GDC-0853 could be exacerbating a background finding in younger animals. Glucose homeostasis was dysregulated following a glucose challenge; however, this occurred only after 28 days of administration and was not directly associated with onset or severity of pancreatic lesions. There were no changes in other common serum biomarkers assessing endocrine and exocrine pancreatic function. Additionally, these lesions were not readily detectable via Doppler ultrasound, computed tomography, or magnetic resonance imaging. Our results indicate that pancreatic lesions in rats are likely a class effect of BTK inhibitors, which may exacerbate an islet-centered pathology that is unlikely to be relevant to humans.

Downloaded from jpet.aspetjournals.org at ASPET Journals on April 18, 2024

JPET Fast Forward. Published on November 7, 2016 as DOI: 10.1124/jpet.116.236224
This article has not been copyedited and formatted. The final version may differ from this version.

4. Introduction

Bruton's tyrosine kinase (BTK) is a cytoplasmic tyrosine kinase in the Tec kinase family (Bmx, Btk, Itk, Rlk, Tec) expressed primarily in hematopoetic cell lineages that has essential functions in B cells and myeloid cells. Antagonism of BTK enzymatic activity in B cells leads to inhibition of B-cell receptor (BCR)-dependent signaling. This results in the disruption of chemotactic signals important for B-cell survival, migration, and proliferation, and a reduction in inflammatory cytokine production from myeloid cells by preventing signaling through the FCγRIII receptor. Small molecule BTK inhibitors are currently being developed for treatment of several hematological cancers and autoimmune diseases.

Ibrutinib (Imbruvica®, Pharmacyclics, Janssen Biotech, Inc.) is a highly effective BTK inhibitor for the treatment of B-cell malignancies that is generally well tolerated and largely devoid of leukopenia and hypogammaglobulinemia. Lymphocytosis is observed clinically with ibrutinib treatment and is thought to be related to inhibition of BCR signaling and efflux of cells from lymphoid tissues into the systemic circulation (Herman et al., 2014). Common adverse events for ibrutinib in patients with chronic lymphocytic leukemia include nausea, vomiting, diarrhea, constipation, petechiae, contusions, atrial fibrillation, and hypertension (Lipsky et al., 2015; Molica, 2015). It is unclear whether any of these findings is directly related to inhibition of BTK activity. Ibrutinib inhibits BTK covalently and irreversibly by targeting a cysteine residue (Cys481) conserved in 10 other kinases within the kinome. Consequently, ibrutinib potently inhibits several "off-target" kinases at therapeutic doses, which may also contribute to the adverse events observed (Evans et al., 2013; Pan et al., 2007). For example, EGFR, TEC, and

Downloaded from jpet.aspetjournals.org at ASPET Journals on April 18, 2024

JPET Fast Forward. Published on November 7, 2016 as DOI: 10.1124/jpet.116.236224
This article has not been copyedited and formatted. The final version may differ from this version.

PI3K-AKT pathway inhibition have been associated with diarrhea, bleeding, and atrial fibrillation, respectively (Byrd et al., 2016; McMullen et al., 2014; Stephens and Spurgeon, 2015).

Loss of BTK function through genetic mutation in humans or knockout (KO) in mice suggests that selective BTK inhibitors should cause suppression of antibody-mediated immune responses while being generally well tolerated in patients. In humans, loss-of-function mutations in the gene encoding BTK result in X-linked agammaglobulinemia (XLA). Due to a block in B-cell development between the pro- and pre-B-cell stage, patients with XLA have a profound reduction in serum immunoglobulin (Ig) concentration of all classes, and fail to mount effective humoral immune responses (Bao et al., 2012; Conley et al., 2000). Patients with XLA are susceptible to recurrent bacterial and enteroviral infections; however, with the advent of Ig infusion therapy, most of them live well into adulthood (Howard et al., 2006). *Btk* KO and X-linked immunodeficient mice have a less severe immunologic phenotype than humans due to only a partial block in B-cell development and some compensation by other BCR signaling components, including TEC kinase (Ellmeier et al., 2000; Kerner et al., 1995; Lindvall et al., 2005; Rawlings et al., 1993). Serum IgG and IgM concentrations in KO mice are reduced but not absent (Satterthwaite et al., 1997). Conversely, serum IgE concentration is increased, which has been attributed to an increase in class-switched B cells in the spleen (Iyer et al., 2011). Moreover, to the extent that BTK deficient humans and mice have been evaluated, few clinical or histopathological abnormalities external to the hematopoetic system have been reported.

Downloaded from jpet.aspetjournals.org at ASPET Journals on April 18, 2024

JPET Fast Forward. Published on November 7, 2016 as DOI: 10.1124/jpet.116.236224
This article has not been copyedited and formatted. The final version may differ from this version.

GDC-0853 is a potent, selective, reversible, small molecule BTK inhibitor in development for the treatment of autoimmune diseases (Young and Crawford, 2016). In preclinical assessments to characterize its toxicity profile, GDC-0853 was well tolerated when orally administered daily to Sprague-Dawley (SD) rats for up to 4 weeks. Findings considered related to pharmacologic activity of GDC-0853 included mild increases in blood lymphocyte count, minimal B-cell depletion in lymphoid organs, and changes in serum Ig concentrations. Unexpectedly, the major finding was pancreatic toxicity, characterized microscopically by multifocal islet-centered hemorrhage, inflammation, fibrosis, and pigment-laden macrophages with adjacent lobular exocrine acinar cell atrophy, degeneration, and inflammation. We conducted comprehensive characterization of the distinct pancreatic lesions associated with GDC-0853 administration in SD rats. Our results suggest that inhibition of BTK enzymatic activity is involved in the pathogenesis of these lesions. The most sensitive strain was SD rat; lesions in Fischer-344 (F-344) and Wistar-Han (WH) rats were of a lesser severity and/or required a longer treatment duration to develop. The observed lesions were histologically similar to spontaneously occurring changes in aging SD rats. Pancreatic lesions were subclinical, with few changes in standard clinical pathology parameters in exocrine or endocrine pancreatic function and were not detectable by imaging techniques. Our results indicate that pancreatic lesions in rats are likely a class effect of BTK inhibitors, which may exacerbate an islet-centered pathology that is unlikely to be relevant to humans.

Downloaded from jpet.aspetjournals.org at ASPET Journals on April 18, 2024

JPET Fast Forward. Published on November 7, 2016 as DOI: 10.1124/jpet.116.236224
This article has not been copyedited and formatted. The final version may differ from this version.

5. Methods

Test articles. All test articles including GDC-0853, GNE-309, ibrutinib, and spebrutinib were synthesized at Genentech, Inc. and formulated for oral administration in the same vehicle: 1.0% (w/v) 4000 cps hydroxypropylmethylcellulose (Fagron; Rotterdam, Netherlands), 0.2% (v/v) Tween 80 (Avantor; Center Valley, PA), and 100 mM citrate buffer (pH 3.0 ± 0.1; Spectrum Laboratory Products, Inc.; New Brunswick, NJ), prepared in reverse osmosis water. The same vehicle served as the control article in the in vivo studies.

Animal care and use. All in vivo experiments were performed in strict accordance with the guidelines in the National Institutes of Health Guide for the Care and Use of Laboratory Animals. All protocols were approved by the Institutional Animal Care and Use Committees at Genentech or Covance, Inc. and appropriate efforts were made to reduce animal suffering. Three strains of rats were used in the in vivo studies: Sprague-Dawley (Crl:SD®[SD]), Wistar-Han (CRL:Crl:WI(Han)), and Fischer-344 (F344 Fischer). Sprague-Dawley rats were obtained from Charles River Laboratories (CRL; Hollister, CA; or Portage, MI). Wistar-Han rats were obtained from CRL (Hollister, CA; or Margate, UK). Fisher-344 rats were obtained from CRL (Kingston, NY). At the start of the studies, animals were 6 to 12 weeks old. Dose formulations (described above) were administered once daily (QD) by oral gavage at a dose volume of 5 or 10 mL/kg. Clinical observations (daily) and body weights (at least twice weekly) were collected for all animals.

Table 1. In vivo study design.

Downloaded from jpet.aspetjournals.org at ASPET Journals on April 18, 2024

JPET Fast Forward. Published on November 7, 2016 as DOI: 10.1124/jpet.116.236224
This article has not been copyedited and formatted. The final version may differ from this version.

Following the initial identification of pancreatic pathological changes in rats administered GDC-0853 in 7- and 28-day toxicity studies, and the absence of similar findings in dogs administered GDC-0853 in a 28-day toxicity study, a series of experiments were conducted in rats to better characterize the pancreas lesions, to determine any strain differences in susceptibility, and to determine whether the developing lesion could be monitored by glucose tolerance testing and/or imaging methods.

Toxicokinetics. Concentrations of test articles in plasma were quantified using liquid chromatography-tandem mass spectrometry (LC-MS/MS) method. Toxicokinetic parameters (C_{max}, T_{max}, and AUC_{0-24}) were determined by non-compartmental methods using the Extravascular input model (Phoenix™ WinNonlin®, version 6.3.0). Concentrations of test articles were also evaluated in pancreas and liver tissue for comparison to concentrations in plasma at the same timepoint.

Clinical pathology. Rats were fasted overnight prior to collection of blood for all clinical pathology measurements. Blood samples for hematology analyses were collected from the retro-orbital plexus under isoflurane-induced anesthesia into ethylenediaminetetraacetic acid (EDTA)-containing tubes and analyzed on a Sysmex XT 2000iV (Sysmex America, Inc., Mundelein, IL). For measurement of IgE and IgG concentrations, blood was collected from the abdominal aorta under isoflurane-induced anesthesia and ketamine into serum separator tubes. Concentration of serum IgE was measured by enzyme-linked immunosorbent assay (ELISA) using mouse anti-rat IgE for capture and detection (Clone B41-1 and Clone B41-3, respectively; BD Biosciences, San Jose, CA) and streptavidin-horseradish peroxidase (HRP; GE Life Sciences, Marlborough, MA). Purified rat IgE isotype control (BD Biosciences, San Jose, CA) was

Downloaded from jpet.aspetjournals.org at ASPET Journals on April 18, 2024

JPET Fast Forward. Published on November 7, 2016 as DOI: 10.1124/jpet.116.236224
This article has not been copyedited and formatted. The final version may differ from this version.

used as a standard. Concentration of serum IgG was measured by ELISA with goat anti-rat IgG-Fc and HRP-conjugated goat anti-rat IgG-Fc as capture and detection antibodies, respectively (Bethyl Laboratories, Montgomery, TX). Rat reference serum (14 mg/mL of rat IgG; Bethyl Laboratories, Montgomery, TX) was used as a standard. Serum amylase, lipase, glucose, and fructosamine were analyzed on blood collected from the jugular vein in conscious rats into serum separator tubes and measured on a Roche PModular Analytics (Roche Diagnostics Corporation, Indianapolis, IN) or on a Beckman Coulter AU680 (Beckman Coulter Inc., West Sacramento, CA) for fructosamine using the manufacturer's applications. Serum insulin was measured by ELISA (Mesoscale Discovery, Gaithersburg, MD).

Histopathology. In all in vivo studies, a necropsy was performed the day following administration of the last dose of test articles. The exception were studies that included a 4-week recovery phase cohort. Pancreas was collected and processed for histopathological evaluation. The tissue was preserved in formalin, embedded in paraffin, and slides were prepared from 5-µm thick sections that were subsequently stained with hematoxylin and eosin. Any macroscopic observations were recorded.

Histochemistry and immunohistochemistry. Formalin-fixed paraffin-embedded sections of pancreas from a subset of control, unaffected, and affected animals administered 30 mg/kg/day GDC-0853 were cut at 4 µm for staining with Masson's Trichrome stain or immunolabeling with antibodies against CD68, clone ED1 (Serotec, Kidlington, UK); cytokeratin 19 (Lifespan Biosciences, Seattle, WA); or smooth muscle actin, clone E184 (Epitomics, Burlingame, CA).

For CD68, sections were deparaffinized and pre-treated for antigen retrieval using Target

Downloaded from jpet.aspetjournals.org at ASPET Journals on April 18, 2024

JPET Fast Forward. Published on November 7, 2016 as DOI: 10.1124/jpet.116.236224
This article has not been copyedited and formatted. The final version may differ from this version.

Retrieval Solution (DAKO, Carpenteria, CA). The slides were subsequently blocked for endogenous peroxidase activity using 3% H_2O_2 and for avidin/biotin using an avidin/biotin blocking kit (Vector Labs, Burlingame, CA). Sections were pre-blocked for non-specific binding sites with blocking buffer. They were then incubated in mouse anti-CD68 at 10 μg/mL, followed by biotinylated horse anti-mouse IgG or biotinylated goat anti-rabbit IgG, respectively (Vector Labs, Burlingame, CA). The sections were incubated in Vectastain ABC Elite reagent (Vector Laboratories; Burlingame, CA), followed by Metal Enhanced DAB (Thermo Scientific; Rockford, IL).

For Cytokeratin 19, after deparaffinization, the sections underwent antigen retrieval in LabVision EDTA, pH 8.0 (Thermo Fisher Scientific; Waltham, MA), blocking, and then incubation in rabbit anti-cytokeratin 19 at 5 μg/mL. The primary antibody was detected with PowerVision Poly anti-Rabbit HRP (Leica, Newcastle, UK), followed by diaminobenzidine (DAB).

For smooth muscle actin, all steps were performed on the Ventana Discovery XT Platform. Sections were deparaffinized using EZ Prep, and pretreatment was accomplished with Cell Conditioner 1 using standard incubation time. Sections were then incubated with rabbit anti-smooth muscle actin at 0.075 μg/mL. The sections were subsequently incubated with anti-Rabbit OmniMap-HRP reagent (Ventana Medical Systems, Tucson, AZ), followed by DAB. All slides were counter stained with hematoxylin, dehydrated, cleared in xylene, and coverslipped.

Glucose tolerance testing. Animals were fasted overnight and administered vehicle or GDC-0853 2 hours prior to OGTT or IVGTT. For the OGTT studies (Days 4, 14, and 32), animals were administered a 50% dextrose solution via oral gavage at a volume of 5

Downloaded from jpet.aspetjournals.org at ASPET Journals on April 18, 2024

JPET Fast Forward. Published on November 7, 2016 as DOI: 10.1124/jpet.116.236224
This article has not been copyedited and formatted. The final version may differ from this version.

mL/kg (total dose of 2500 mg/kg dextrose). Blood (approximately 0.25 mL) was collected prior to administration of GDC-0853 and dextrose and at 15, 30, 60, and 120 minutes after administration of dextrose. Blood samples were collected via the tail vein (Days 4 and 14) or jugular vein (Day 32) onto a glucometer (Days 4 and 14: Nova StatStrip; Nova biomedical, Waltham, MA; Day 32: AlphaTRAK2; VWR, Radnor, PA) for analysis of blood glucose level. The remaining blood was processed to plasma for analysis of insulin levels. For the IVGTT study (Days 4, 14, and 28), rats were cannulated in femoral artery. Animals were intravenously administered a 50% dextrose solution via tail vein at a volume of 5 mL/kg (total dose of 2500 mg/kg dextrose). Whole blood (0.1 mL) was collected prior to and at 2, 5, 10, 15, 30, and 60 minutes after administration of dextrose. Blood samples were collected via the tail vein onto a Nova StatStrip glucometer for analysis of blood glucose level. The remaining blood was processed to plasma for analysis of insulin levels.

Ultrasound imaging study. Micro-ultrasound imaging was performed with the Visualsonics Vevo2100 micro-imaging system (Toronto, Ontario, Canada) after 7 and 14 days of administration of vehicle, GNE-309, or GDC-0853. Pancreatic images were obtained with an MS400 256-element array transducer (30 MHz center frequency), 12 mm field-of-view (FOV), axial resolution of 0.04 mm, and lateral resolution of 0.1 mm. Three-dimensional pancreatic images were acquired with a motorized drive mechanism that traverses the z-axis while acquiring x-y axis images at regular spatial intervals of 0.05 mm. Both b-mode and power Doppler (PD) images were acquired. Average b-mode intensity (in arbitrary units) for the pancreas was obtained from a single imaging slice that contains the largest transverse region of pancreas. Power Doppler images for the

Downloaded from jpet.aspetjournals.org at ASPET Journals on April 18, 2024

JPET Fast Forward. Published on November 7, 2016 as DOI: 10.1124/jpet.116.236224
This article has not been copyedited and formatted. The final version may differ from this version.

same slice were used to estimate percent vascularity [(PD vascular area/total pancreatic area) × 100].

Computed tomography imaging study. A GE Healthcare eXplore Ultra small animal CT scanner was used to scan the pancreas at baseline (Day -1) and after 7 and 14 days of administration of vehicle or GDC-0853. To attain dynamic contrast enhancement, a bolus of 0.6 mL Iohexol (Omnipaque-300) was administered via lateral tail vein at a rate of 7.2 mL/sec with a delay of 5 seconds before beginning the scan. Regions of interest were generated for the head, body, and tail of pancreas as well as for abdominal aorta, liver, and portal vein to calculate the following parameters:

- Time-attenuation curve
- Pancreatic enhanced and unenhanced phases
- Hepatic enhanced and unenhanced phases
- Functional perfusion data: blood volume (mL), blood flow (mL/min), mean transit time (min), and permeability (mL/100 g of tissue/min)

The ratio of the late to early enhancement obtained from the hepatic and pancreatic phases (L:E) was quantified. For a healthy human with no pancreatic disease, the L:E ratio is ≤ 1 (Hashimoto et al., 2011).

Magnetic resonance imaging study. Magnetic resonance imaging was conducted after 7 days (4 males from each group on Day 8, and 4 males from each group on Day 9) and 14 days (Day 15 or 16) of administration of vehicle or GNE-309. Experiments were performed on a 4.7T horizontal imaging system (Agilent Technologies, Santa Clara, CA) using a 63 mm quadrature volume coil. The transverse relaxation time T_2 was measured using a 2D multi-slice fast spin echo experiment with FOV 60 × 60 mm^2, 16 coronal

Downloaded from jpet.aspetjournals.org at ASPET Journals on April 18, 2024

JPET Fast Forward. Published on November 7, 2016 as DOI: 10.1124/jpet.116.236224
This article has not been copyedited and formatted. The final version may differ from this version.

slices of 1.0-mm thickness, matrix size 128 × 128 (zero-filled to 256 × 256), echo train length (ETL) 16, four echo times (TE) of 7, 16, 26, and 36 msec, and 4 averages. Data acquisition was synchronized with respiration by triggering off the respiration signal produced by the SA Instruments equipment, which resulted in a repetition time (TR) of approximately 2000 msec. For each image pixel, T_2 and S_0 were determined by fitting to the equation:

$$S(TE)=S_0 \exp\left(-\frac{TE}{T_2}\right)$$

$$\left(-\frac{TE}{T_2}\right)-\frac{TE}{T_2}$$

T_2, or transverse relaxation time, is the decay constant for the component of magnetization that is perpendicular to the static magnetic field of magnet, S_0. The pancreas was manually outlined on the S_0 image. The volume and average T_2 of the pancreas was calculated. Pancreatic lesions could lead to an increase in volume or T_2 due to neoplasm, inflammation, or edema or a decrease in T_2 due to hyper-dense tissue (hyperplasia).

Kinase panel selectivity testing. GDC-0853, GNE-309, and ibrutinib were tested at a concentration of 1 μM against a panel of 221 recombinant human kinase biochemical assays, including cytoplasmic and receptor tyrosine kinases, serine/threonine kinases, and lipid kinases (Invitrogen SelectScreen Kinase Profiling Services, Thermo Fisher Scientific, Waltham, MA). For kinase activity assays, the ATP concentrations used were within 2-fold of the apparent Michaelis constant (K_m) for each kinase, while for ATP-site competition binding assays the active site competitive probe concentration used was approximately equal to its dissociation constant (K_d).

Downloaded from jpet.aspetjournals.org at ASPET Journals on April 18, 2024

JPET Fast Forward. Published on November 7, 2016 as DOI: 10.1124/jpet.116.236224
This article has not been copyedited and formatted. The final version may differ from this version.

Human ex vivo whole blood CD69 assay. Heparinized whole blood (100 µL) from healthy human volunteers in 96-well square top/tapered V-bottom deep-well plates (Analytical Sales, Pompton Plains, NJ) was incubated for 1 hour at 37°C with a titration of BTK inhibitor or vehicle in duplicate (0.38% dimethyl sulfoxide (DMSO). Blood was then stimulated with 50 µg/mL of goat anti-human IgM $F(ab')_2$ (Southern Biotech, Birmingham, AL). After an 18-hour incubation, cells in the blood were stained with 45 µL per well of a cocktail containing anti-mouse CD19-PerCP-Cy5.5, clone SJ25C1 (1.1 µg/mL; BD Biosciences, San Jose, CA), anti-mouse CD27-FITC, clone L128 (0.18 µg/mL; BD Biosciences, San Jose, CA), and anti-mouse CD69-PE, clone FN50 (7.5 µL per 45 µL cocktail; BD Pharmingen, San Jose, CA) or PE mouse IgG1, κ isotype control (10 µL per 45 µL cocktail; BD Pharmingen, San Jose, CA) for 30 minutes at room temperature. This was followed by lysis of red blood cells using 1× BD Pharm lysis buffer (BD Biosciences, San Jose, CA). Cells were washed with FACS buffer and fixed with 2% paraformaldehyde. Samples were acquired and analyzed on a BD LSRII flow cytometer. Activation of B cells ($CD19^+CD27^-$) was assessed based on CD69 PE mean fluorescence intensity (MFI) using FACSDiva software (BD Biosciences, San Jose, CA). The CD69 PE MFI was plotted against the $\log_{10}$ of the BTK inhibitor concentration and fit by non-linear regression using Prism v5.0 (GraphPad software, La Jolla, CA) to the variable slope 4-parameter sigmoidal inhibition equation to determine the half-maximal inhibitory concentration (IC_{50}). Inhibitors were tested against blood from at least 3 different donors, and the mean IC_{50} (± SD) was calculated.

Human ex vivo whole blood phospho-BTK assay. Heparinized whole blood (304 µL) from healthy human volunteers in 96-well square top/tapered V-bottom deep-well plates

Downloaded from jpet.aspetjournals.org at ASPET Journals on April 18, 2024

JPET Fast Forward. Published on November 7, 2016 as DOI: 10.1124/jpet.116.236224
This article has not been copyedited and formatted. The final version may differ from this version.

was incubated for 6 hours at 37°C with a titration of BTK inhibitor or vehicle in duplicate (8% DMSO) in a water reservoir within a tissue culture incubator (0.4% DMSO). After the incubation, the plate was put on ice and the blood was diluted with 320 µL of 2× Lysis Buffer (Cell Signaling Technology, Danvers, MA) containing complete protease inhibitors (Roche Diagnostics, Indianapolis, IN), 2× phosphatase inhibitor cocktails 2 and 3 (Sigma, St. Louis, MO), and 200 µM sodium orthovanadate (New England Biolabs, Ipswich, MA). The diluted blood was thoroughly mixed and the plate was sealed and stored at –80°C. For pBTK(Y223) detection, High Bind 96-well plates (Meso Scale Discovery, Gaithersburg, MD) were spotted with 10 µL per well of 10 µg/mL mouse anti-BTK monoclonal antibody (BD Biosciences, San Jose, CA) then allowed to dry before use. Phospho-BTK from 250 µL of thawed lysate was detected using rabbit anti-human pBTK(Y223) monoclonal antibody (13.2 µg/mL; Epitomics, Burlingame, CA) and SULFO-TAG conjugated goat anti-rabbit IgG antibody (1 µg/mL; Meso Scale Discovery, Gaithersburg, MD). The electrochemiluminescence (ECL) signal was recorded with a SECTOR Imager 6000 MSD reader (Meso Scale Discovery, Gaithersburg, MD). The pBTK ECL signal was plotted against the $\log_{10}$ of the inhibitor concentration and fit by non-linear regression using Prism v5.0 (GraphPad software, La Jolla, CA) to the variable slope 4-parameter sigmoidal inhibition equation to determine the IC_{50}. Inhibitors were tested against blood from at least 3 different donors, and the mean IC_{50} (± SD) was calculated.

Expression of Btk in pancreas. Laser capture microdissection caption microscopy (LCM) was conducted on exocrine and endocrine tissue from SD rat pancreatic tissue (3 samples) using Zeiss Palm (Thornwood, NY). RNA was isolated using the Arcturus

Downloaded from jpet.aspetjournals.org at ASPET Journals on April 18, 2024

JPET Fast Forward. Published on November 7, 2016 as DOI: 10.1124/jpet.116.236224
This article has not been copyedited and formatted. The final version may differ from this version.

PicoPure kit (Applied Biosystems, Carlsbad, CA) and DNase treated on-column before bioanalyzer quantification and qualification (Agilent RNA 6000 Pico Kit, Santa Clara, CA). Reverse transcription to cDNA (SuperScript® VILO™ Master Mix; Thermo Fisher Scientific, Waltham, MA) was subsequently performed on the LCM samples: human islet RNA (4 anonymous samples, sex unknown; Prodo Labs, Irvine, CA), universal RNA (rt/hu; Clontech, Mountain View, CA), and total RNA from pooled isolated rat islet preparations (AllCells, Alameda, CA). This was followed by pre-amplification utilizing PreAmp Master Mix (Fluidigm, South San Francisco, CA). Subsequent PCR reactions for relative gene expression utilized Taqman Fast Universal PCR Master Mix (Applied Biosystems, Waltham, MA) and the 96.96 Dynamic Array™ IFC (Fluidigm, South San Francisco, CA) on the Biomark™ HD System (Fluidigm, South San Francisco, CA). All target and housekeeping gene assays used for pre-amplification and relative gene expression were species-specific Taqman® Assays purchased from Life Technologies (Waltham, MA). Non-blank values in all samples were all detectable with a good dynamic range, and there were no false positives in any assay blanks. Standard curves from diluted islet samples were within linear range for robust assay detection. Finally, gene expression was normalized against the ribosomal endogenous control gene, 18S. Data are represented as delta CTs, relative to the highly-expressed 18S, where negative numbers are lower than 18S and positive numbers are greater than 18S.

Statistical analyses. Data are expressed as mean ± standard deviation. A repeated-measures models were fitted to the longitudinal blood glucose and insulin data with treatment, timepoints, and their interaction as fixed effects and animal as a random effect. Evaluation of effect of treatment on change from baseline was conducted at each

Downloaded from jpet.aspetjournals.org at ASPET Journals on April 18, 2024

JPET Fast Forward. Published on November 7, 2016 as DOI: 10.1124/jpet.116.236224
This article has not been copyedited and formatted. The final version may differ from this version.

timepoint using contrast t-test with Bonferroni correction for multiple comparisons. Log transformation was applied prior to analysis to address heteroskedasticity where appropriate.

Levene's test was used to test for heteroskasticity in b-mode intensity and percent vascularity for US and MRI T_2 data. If Levene's test was significant, treatment effect was evaluated using Welch's t-test; otherwise, a 2-sample t-test assuming equal variances was conducted.

For all comparisons, statistical analyses were evaluated at 5% significance level and statistical analysis of data was performed using SAS 9.2.

For the CT study, differences in-between animals administered GDC-0853 or vehicle were tested using a t-test with $P < 0.05$ in the statistical package.

For the MRI study, differences in volume or overall pancreatic T_2 between animals administered GNE-309 or vehicle were tested using a t-test with $P < 0.05$ in the statistical package JMP (SAS institute).

Downloaded from jpet.aspetjournals.org at ASPET Journals on April 18, 2024

JPET Fast Forward. Published on November 7, 2016 as DOI: 10.1124/jpet.116.236224
This article has not been copyedited and formatted. The final version may differ from this version.

6. Results

BTK inhibitors induce distinct pancreatic lesions in Sprague-Dawley rats

Figure 1. Pancreatic histopathology in Sprague-Dawley rats administered GDC-0853.

Table 2. Comparison of BTK inhibitors and results in SD rats: toxicokinetics, BTK potency, kinase selectivity, and incidence of pancreatic lesions.

GDC-0853, a potent, selective, reversible, small molecule BTK inhibitor was orally administered to SD rats for 1 to 28 consecutive days at doses up to 100 mg/kg/day. Exposure to GDC-0853 (assessed by maximal concentration (C_{max}) and area under the concentration-time curve from time 0 to 24 hours (AUC_{0-24})) increased over the dose range tested. Generally, increase in exposure was dose-proportional up to 30 mg/kg/day and greater than dose-proportional between 30 and 100 mg/kg/day. No toxicologically significant accumulation or sex-dependent differences in exposure was observed (Table 2 and Supplemental Figure 1). GDC-0853 was generally well tolerated. Occasional hypoactivity, reduced mean body weight gain, and reduced food consumption (approximately 80% of control means) were observed only after 28 days at the highest dose tested, 100 mg/kg/day.

GDC-0853-related changes in clinical pathology parameters included mildly increased blood lymphocyte counts (up to 50% over control mean) and elevated serum IgE concentration (up to 5-fold over control mean) with no clear change in IgG concentration (Supplemental Figure 2). These changes were consistent with reported effects of BTK inhibition following administration of ibrutinib or through loss of function in KO mice

Downloaded from jpet.aspetjournals.org at ASPET Journals on April 18, 2024

JPET Fast Forward. Published on November 7, 2016 as DOI: 10.1124/jpet.116.236224
This article has not been copyedited and formatted. The final version may differ from this version.

(Herman et al., 2014; Iyer et al., 2011; Satterthwaite et al., 1997).

GDC-0853-related microscopic findings in the pancreas were observed at doses ≥ 5 mg/kg/day after dosing durations of 7 to 28 days. Multifocal pancreatic lesions, often islet-centered but sparing islet cells, were characterized by varying degrees (minimal-to-moderate) of islet/peri-islet hemorrhage, fibrosis, mixed cell infiltrates, and pigment-laden macrophages. Additionally, significant involvement of adjacent exocrine acinar tissue was noted in some animals, consisting of lobular acinar cell atrophy with acinar cell degeneration/apoptosis, interstitial mixed cell (predominantly macrophages with fewer lymphocytes and neutrophils) infiltrates, and/or interlobular hemorrhage and edema. Despite substantial involvement of islet tissue, there was little microscopic evidence of islet cell degeneration. Pancreatic lesions were not observed in rats administered 30 mg/kg/day GDC-0853 for 1 or 3 days, suggesting the onset of the lesion was between 4 and 7 days of dosing. Representative photomicrographs depicting the variety of pancreatic findings present are presented in Figure 1. The most subtle microscopic change was minimal hemorrhage in the small blood vessels of the peri-islet vasculature at the interface of the islet and exocrine tissue (Figure 1A). In more severely affected islets, the hemorrhage was more extensive, and islet/peri-islet lesions had the appearance of “exploding islets” with clusters or individual islet cells floating in lakes of hemorrhage and fibrin and secondary degeneration of adjacent exocrine acinar cells and varying amounts of mixed cell inflammatory infiltrates and pigment-laden macrophages (Figure 1B). Other islets were surrounded and/or dissected by large areas of dense fibroplasia and fibrosis (Figure 1C). Atrophy of adjacent lobules of exocrine pancreas was suggestive of impaired blood flow through the affected peri-islet vasculature.

Downloaded from jpet.aspetjournals.org at ASPET Journals on April 18, 2024

JPET Fast Forward. Published on November 7, 2016 as DOI: 10.1124/jpet.116.236224
This article has not been copyedited and formatted. The final version may differ from this version.

Multifocal lesions at different stages of development were often present in the same animal, suggesting an ongoing insult (Figure 1D). Pancreatic lesions were not observed in any animal treated with vehicle or 0.5 mg/kg/day GDC-0853 for up to 28 days. Thus, 0.5 mg/kg GDC-0853 was considered to be the no-observed-adverse-effect-level (NOAEL) for this finding. There was considerable resolution of the pancreatic pathology at the end of a 28-day recovery period, with only small amounts of mature fibrous connective tissue dissecting islet/peri-islet areas and pigment-laden macrophages in the interstitial and interlobular connective tissue remaining.

Immunohistochemical and histochemical evaluation of the pancreatic lesion was performed to further characterize the pathologic changes observed microscopically by hematoxylin and eosin staining. Histochemical staining of the affected pancreatic sections with Masson's trichrome stain demonstrated an increase in blue-staining collagen fibers consistent with fibrosis within affected islet/peri-islet and interstitial areas (Figure 1E). Increased smooth muscle actin labeling within areas of pancreatic islet/peri-islet fibrosis could originate from several different cell types including blood vessel-associated smooth muscle pericytes or a localized activation of pancreatic stellate cells (Figure 1F). Increased CD68 labeling confirmed a macrophage infiltrate (Figure 1G). Increased numbers of weakly cytokeratin 19-positive tubular structures were present in surrounding areas of islet/peri-islet fibrosis and within atrophic exocrine lobules. This was consistent with pancreatic ductular proliferation and/or formation of duct-like tubular complexes by atrophic acinar cells (Figure 1H). These findings confirmed the presence of fibrosis and a CD68-positive macrophage infiltrate and suggested that blood vessel-associated pericytes or activated pancreatic stellate cells may

Downloaded from jpet.aspetjournals.org at ASPET Journals on April 18, 2024

JPET Fast Forward. Published on November 7, 2016 as DOI: 10.1124/jpet.116.236224
This article has not been copyedited and formatted. The final version may differ from this version.

be involved in the production of the fibroplastic reaction.

Figure 2. Molecular structures of GDC-0853, GNE-309, ibrutinib, and spebrutinib.

Figure 3. Exposure to GDC-0853 in Sprague-Dawley rats relative to BTK (on-target) and off-target (BMX, FGR, SRC) kinase half-maximal inhibitory concentrations.

To help understand whether inhibition of BTK enzyme activity was driving the SD rat pancreatic pathologic changes, we evaluated 3 additional BTK inhibitors in SD rats: GNE-309, ibrutinib, and spebrutinib (Figure 2). GNE-309 is a potent and highly selective BTK inhibitor that is structurally-related to GDC-0853. Ibrutinib and spebrutinib are structurally-distinct, potent, and less selective BTK inhibitors. In contrast to GDC-0853, which reversibly inhibits BTK at the ATP binding site, ibrutinib and spebrutinib inhibit BTK covalently and irreversibly by targeting a cysteine residue (Cys481) near the ATP binding site that is conserved in 10 other kinases within the kinome (Evans et al., 2013; Pan et al., 2007). As a consequence, covalent-binding BTK inhibitors potently inhibit many of these “off-target” kinases.

The on-target potency of the 4 molecules was compared using 2 human ex vivo whole blood assays to evaluate BTK-pathway inhibition. Additionally, the selectivity was assessed using a panel of 221 in vitro kinase assays, including cytoplasmic and receptor tyrosine kinases, serine/threonine kinases, and lipid kinases. This single point testing at 1 μM showed that, relative to ibrutinib and spebrutinib, GDC-0853 and GNE-309 were much more selective for BTK over other kinases (Table 2). GDC-0853 and GNE-309 were also evaluated in a broad panel of biochemical radioligand-binding and enzyme

Downloaded from jpet.aspetjournals.org at ASPET Journals on April 18, 2024

JPET Fast Forward. Published on November 7, 2016 as DOI: 10.1124/jpet.116.236224
This article has not been copyedited and formatted. The final version may differ from this version.

assays, including 42 targets of major classes of biogenic amine receptors, neuropeptide receptors, ion channel-binding, and neurotransmitter transporter. The results of these assays did not reveal any significant off-target binding (data not shown).

Doses of GNE-309, ibrutinib, and spebrutinib were selected at levels that would result in clinically relevant plasma exposures (Pharmacyclics, Inc., 2015; Brown et al., 2016). When administered to SD rats for 7 to 14 consecutive days, exposure to each of the molecules (C_{max} and AUC_{0-24}) increased with the dose over the dose range tested (Table 2). All molecules were well tolerated with no clinical signs or body weight changes attributed to treatment. Microscopic pancreatic lesions similar to those observed in SD rats administered GDC-0853 were present with GNE-309, ibruinib, and spebrutinib at all dose levels examined, but not in animals treated with vehicle (Table 2).

Taken together with the highly selective properties of GDC-0853, where no off-target kinase activity is expected at the low-observed-adverse-effect-level (LOAEL) for pancreatic lesions in SD rats (7 days at 5 mg/kg/day), these data indicate that inhibition of BTK enzymatic activity in SD rats is likely involved in development of the pancreatic lesions (Figure 3).

Sprague-Dawley rat was the most sensitive strain tested

Figure 4. Strain sensitivity to BTK inhibitor-induced pancreatic lesions

During the histopathologic characterization of the GDC-0853-related pancreatic lesions, it was noted that the more mildly affected pancreatic islets in young (10- to 12-week-old) SD rats treated with GDC-0853 closely resembled the microscopic changes of the

Downloaded from jpet.aspetjournals.org at ASPET Journals on April 18, 2024

JPET Fast Forward. Published on November 7, 2016 as DOI: 10.1124/jpet.116.236224
This article has not been copyedited and formatted. The final version may differ from this version.

age-related spontaneous pancreatic islet hemorrhage and fibrosis in SD rats (Dillberger, 1994; Imaoka et al., 2007; Reaven and Reaven, 1981). This similarity suggested that BTK inhibitors might be exacerbating a background pancreatic change in younger SD rats and that the SD strain may be highly sensitive to the pancreatic effects of GDC-0853. In order to test this hypothesis, we investigated the effects of BTK inhibitors on the pancreas of 2 other commonly used laboratory rat strains, F-344 and WH. Following administration of GDC-0853 (30 mg/kg/day) or GNE-309 (100 mg/kg/day) for 14 consecutive days, exposure was confirmed in all treated animals. Plasma concentrations of GDC-0853 and GNE-309 were each similar across strains at 3 hours post-dose, near the anticipated time to maximal concentration (T_{max}), on Day 14 (Figure 4). With both molecules, the same incidence and severity of BTK inhibitor-related pancreatic lesions was observed across the strains: in 5 of 6 SD (moderate), 1 of 6 F-344 (minimal), and 0 of 6 WH rats. Thus, SD rats were particularly sensitive to the effects of BTK inhibitors on the pancreas (Figure 4). The reduced sensitivity of WH rats was further confirmed in longer term studies with GDC-0853. No GDC-0853-related pancreatic lesions were observed in WH rats administered GDC-0853 at doses up to 30 mg/kg/day for 28 days. Following 6 months of daily dosing up to 30 mg/kg/day in WH rats, however, minimal-to-mild pancreatic islet/peri-islet fibrosis and pigment-laden macrophages were observed in males administered ≥ 2 mg/kg/day GDC-0853 (data not shown). These pancreatic changes were similar in extent and severity to the islet changes occurring spontaneously in aging SD rats, but did not occur in any vehicle-treated animals and therefore were considered related to GDC-0853 administration.

BTK is expressed at low levels in the rat and human pancreas

Downloaded from jpet.aspetjournals.org at ASPET Journals on April 18, 2024

JPET Fast Forward. Published on November 7, 2016 as DOI: 10.1124/jpet.116.236224
This article has not been copyedited and formatted. The final version may differ from this version.

Figure 5. BTK is expressed at low levels in endocrine and exocrine tissue from rat and human pancreas.

BTK is predominantly expressed in most hematopoietic cells and tissues harboring these cell types. To date, there is no reported expression or function of BTK in endocrine or exocrine pancreas. To better understand whether BTK enzyme inhibition in the pancreas itself could be causing the lesions in rats, we evaluated local drug concentrations of GDC-0853 and Btk expression in pancreatic tissue. Following 21 days of dosing at 30 mg/kg in SD rats, GDC-0853 concentration near T_{max} (3 hours post-dose) in plasma (8.12 µM) was greater than in pancreas (0.319 µM) or liver (2.44 µM). This confirmed local exposure but demonstrated no preferential drug accumulation in pancreas and liver. Transcriptional profiling of Btk was performed on laser-captured microdissected endocrine and exocrine tissue from SD rats and purchased human islet samples. Compared to lymph node or universal RNA samples, Btk was expressed at significantly lower levels across islet/endocrine and exocrine tissue from both rat and human (Figure 5). It is not known whether these Btk transcripts would translate to protein expression.

BTK inhibition has mild effects on glucose metabolism

Figure 6. Amylase, lipase, insulin, and fructosamine levels in Sprague-Dawley rats following administration of GDC-0853.

Figure 7 Glucose and insulin levels in Sprague-Dawley rats following administration of

Downloaded from jpet.aspetjournals.org at ASPET Journals on April 18, 2024

JPET Fast Forward. Published on November 7, 2016 as DOI: 10.1124/jpet.116.236224
This article has not been copyedited and formatted. The final version may differ from this version.

GDC-0853.

After administration of GDC-0853 to SD rats at doses up to 100 mg/kg/day for 28 consecutive days, despite the presence of pancreatic lesions, there were no changes in serum biomarkers of exocrine and endocrine pancreatic function, including amylase, lipase, insulin, or fructosamine (Figure 6A-D). There was a mild increase in blood glucose (10% to 30%, $P < 0.05$) in fasted rats administered 100 mg/kg/day GDC-0853 after 12 and 28 days of dosing (Figure 7A); however, given that pancreatic lesions of a similar incidence and severity were observed in animals administered ≥ 10 mg/kg/day in this study, the relationship between fasted blood glucose levels and pancreatic lesions was uncertain. An oral glucose tolerance test (OGTT) was performed as a more sensitive test of subclinical effects on glucose homeostasis. At 28 days, there was an increased and prolonged peak in blood glucose (without corresponding changes in insulin) relative to animals administered vehicle at ≥ 10 and ≥ 30 mg/kg/day GDC-0853, respectively (Figure 7B-C). In order to evaluate the effectiveness of the OGTT as a premonitory endpoint in predicting the onset of the pancreatic changes, a subsequent study evaluated the effects of 10 and 100 mg/kg/day GDC-0853 after 4 and 14 days of administration. At these earlier time points, there were no differences between animals treated with vehicle and GDC-0853 in the OGTT response of blood glucose or serum insulin, despite the presence of pancreatic lesions in the majority of animals administered GDC-0853 (9 of 12) at 14 days. An intravenous glucose tolerance test (IVGTT) in SD rats administered 30 mg/kg/day GDC-0853 evaluated at 4, 14, and 28 days of dosing showed minor changes only after 28 days (Supplemental Figure 3). Collectively, these findings show

Downloaded from jpet.aspetjournals.org at ASPET Journals on April 18, 2024

JPET Fast Forward. Published on November 7, 2016 as DOI: 10.1124/jpet.116.236224
This article has not been copyedited and formatted. The final version may differ from this version.

that GDC-0853 administration results in mild glucose dysregulation after prolonged treatment in rats. This effect is not clearly related to the pancreatic lesions; therefore, fasted glucose or glucose challenge tests are not biomarkers of BTK-related pancreatic toxicity in SD rats.

Doppler ultrasound, computed tomography, and magnetic resonance imaging were not adequately sensitive to identify BTK inhibitor-related pancreatic pathologic changes in vivo

Figure 8. Ultrasound imaging of the pancreas in Sprague-Dawley rats following administration of GNE-309 or GDC-0853.

Histopathologic characterization of the BTK inhibitor-related pancreatic changes in SD rats identified hemorrhage, edema, and fibrosis as the major structural alterations. We employed several clinically-relevant imaging techniques to determine whether the pancreatic changes in SD rats could be visualized in vivo in order to evaluate their potential application as a clinical monitoring tool.

In the studies evaluating US, GDC-0853 (30 mg/kg/day) or GNE-309 (100 mg/kg/day) was orally administered to male SD rats for 14 days and imaging was performed on Days 7 and 14. Histopathologic evaluations at the Day 15 necropsy confirmed pancreatic lesions in 7 of 8 and 8 of 8 animals administered GDC-0853 and GNE-309, respectively. There were no significant differences detected by b-mode intensity or percent vascularity parameters after 7 days of treatment with either molecule. After 14 days of treatment, b-mode intensity and percent vascularity were significantly elevated over the respective

Downloaded from jpet.aspetjournals.org at ASPET Journals on April 18, 2024

JPET Fast Forward. Published on November 7, 2016 as DOI: 10.1124/jpet.116.236224
This article has not been copyedited and formatted. The final version may differ from this version.

controls for animals treated with GNE-309 but not GDC-0853 (Figure 8). Together with the lack of association between individual severity of pancreatic findings and these parameters, a consistent relationship to the histological changes could not be supported. CT and MRI evaluations were conducted following administration of GDC-0853 or GNE-309 for 14 or 17 days, respectively. Pancreatic lesions were confirmed in all treated animals. The CT imaging demonstrated no clear GDC-0853-related effects detected by time-attenuation curve and L/E ratio, pancreatic enhanced and unenhanced phases, or functional perfusion (Supplemental Figure 4). Similarly, there were no clear treatment-related changes in MRI T_2 maps (Supplemental Figure 5).

Downloaded from jpet.aspetjournals.org at ASPET Journals on April 18, 2024

JPET Fast Forward. Published on November 7, 2016 as DOI: 10.1124/jpet.116.236224
This article has not been copyedited and formatted. The final version may differ from this version.

7. Discussion

In these experiments we showed that administration of a selective BTK small molecule inhibitor, GDC-0853, to SD rats results in distinct microscopic pancreatic lesions characterized by multifocal islet/peri-islet hemorrhage, inflammation, fibrosis, and pigmented macrophages with adjacent lobular exocrine acinar cell atrophy, degeneration, and inflammation. These lesions demonstrated significant reversibility following a 4-week recovery period, with only mature islet/peri-islet fibrosis and pigmented macrophages remaining. Additional BTK inhibitors – 2 structurally distinct, irreversible inhibitors ibrutinib and spebrutinib and a second highly selective, reversible inhibitor GNE-309 – caused the same pancreatic lesions when administered to SD rats under the same conditions. For the selective BTK inhibitors, the pancreatic lesions were observed at doses where no significant off-target activity was expected. Collectively, these data strongly suggest that inhibition of BTK enzymatic activity is involved in the pathogenesis of these lesions, which may be considered a class effect of BTK inhibitors in rats.

As evidence of species specificity, no similar pancreatic findings were observed in CD-1 mice or Beagle dogs administered GDC-0853 or other potent BTK inhibitors for up to 9 months, despite achieving exposures up to 24-times the established LOAEL in SD rats (Supplemental Figure 6). In addition, there are no reports of pancreatic changes in mice with BTK mutations (knockout or XID) or pancreatic disease or dysfunction in male patients who lack functional BTK enzyme (XLA) in at least 6 published clinical series and/or registries including more than 400 patients (Aghamohammadi et al., 2006; Hermaszewski and Webster, 1993; Lederman and Winkelstein, 1985; Moin et al., 2004; Plebani et al., 2002; Winkelstein et al., 2006). Also of note, ibrutinib has been

Downloaded from jpet.aspetjournals.org at ASPET Journals on April 18, 2024

JPET Fast Forward. Published on November 7, 2016 as DOI: 10.1124/jpet.116.236224
This article has not been copyedited and formatted. The final version may differ from this version.

administered to thousands of patients and is not associated with pancreatic toxicity. Although SD rats were the most sensitive strain tested in the current studies, F-344 and WH rats developed BTK inhibitor-related pancreatic changes of a lesser severity after 2 weeks or 6 months, respectively. Taken together, these results support the hypothesis that biological differences predispose rats to BTK inhibitor-induced pancreatic changes with the SD rat being an exceptionally sensitive strain. Furthermore, the likelihood of clinical translatability is low.

Spontaneous pancreatic islet hemorrhage and fibrosis in SD rats is well described (Dillberger, 1994; Imaoka et al., 2007; Reaven and Reaven, 1981). The changes are characterized by an initial extravasation of red blood cells from the peri-islet capillaries and hemosiderin (pigment) deposition in the center or periphery of the islet. The earliest observations have been recorded in 12-week old animals, but the incidence and severity of the changes increase considerably by 26 weeks of age (Imaoka et al., 2007). These spontaneous islet changes are more commonly observed in males, and a similar sex predilection for males was observed in the GDC-0853-related pancreatic findings. The relative sex- and strain-susceptibility differences may be related to body weight gain and overall metabolic status. Male SD rats have a significantly faster growth rate compared to male WH rats, owing to higher daily food consumption. At 12 weeks of age, male SD rats are already 30% to 70% larger than male WH rats (Hayakawa et al., 2013; Charles River Laboratories International, Inc.). Reducing body weight by exercise and/or caloric restriction (from 800 to 500 g at 12 months of age) significantly reduced the incidence of spontaneous pancreatic islet pathologic changes when compared with sedentary SD rats fed ad libitum (Reaven and Reaven, 1981). SD rats have higher rates of hyperglycemia

Downloaded from jpet.aspetjournals.org at ASPET Journals on April 18, 2024

JPET Fast Forward. Published on November 7, 2016 as DOI: 10.1124/jpet.116.236224
This article has not been copyedited and formatted. The final version may differ from this version.

and a higher predisposition to streptozotocin-induced diabetes. These findings may be associated with strain differences in the developing islet (Ojiro et al., 1993). Pancreatic islet pathology observed in rat strains with a genetic predisposition to obesity/diabetes suggests that rats are sensitive to developing islet hemorrhage in response to increased metabolic demands. Spontaneous pancreatic islet changes in the OLETF, WY/Kob, ZDF, and Goto-Kakizaki rats (Jones et al., 2010; Katsuda et al., 2014; Lacraz et al., 2009) appear to be related to increased insulin demand and hyperinsulinemia. They commonly include early islet hypertrophy/hyperplasia and degranulation of beta cells, followed by hemorrhage, hemosiderin deposition, inflammation and/or fibrosis. Evidence of vascular injury in response to increased metabolic demand, including hemorrhage and hemosiderin deposition, appears to be unique to rats. In mouse models of type 2 diabetes and in human patients with type 2 diabetes, islet changes have been observed that include beta cell hyperplasia followed by decreased beta cell mass, amyloid deposition, and inflammation; but, notably, hemorrhage has not been reported as a feature characterizing the pancreatic pathology (Bonner-Weir and O'Brien, 2008; Donath et al., 2008; Hull et al., 2005; Iizuka et al., 2005; Junger et al., 2002; Talchai et al., 2009). Compared with mice and other mammals including dogs and primates, rats have unique anatomical features within the microvasculature perfusing the endocrine and exocrine tissue (Greaves, 2012), which may be associated with increased susceptibility to injury.

The spontaneous pancreatic islet lesions observed in SD rats are thought to be preceded by alterations in glucose metabolism. In contrast, GDC-0853-treated SD rats do not have significantly altered glucose metabolism at the early stages of development of lesion, indicating that the BTK inhibitor-induced pancreatic changes likely involve a distinct

Downloaded from jpet.aspetjournals.org at ASPET Journals on April 18, 2024

JPET Fast Forward. Published on November 7, 2016 as DOI: 10.1124/jpet.116.236224
This article has not been copyedited and formatted. The final version may differ from this version.

pathogenic mechanism. In the acute-stage, occurring within as few as 7 days of administration of GDC-0853, pancreatic pathology was characterized by islet/peri-islet hemorrhage, suggesting drug-induced microvascular injury to the thin-walled capillaries within this region. A similar hypothesis was suggested by Brennenman et al. (Brenneman et al., 2014), who described a very similar drug-related pancreatic finding in SD rats for which the drug target was not disclosed. In their investigations, an increase in immunohistochemical markers of endothelial cytotoxicity in the islet microvasculature between 1 and 5 days of administration was identified. This was suggestive of test article-induced vascular injury, although it was acknowledged that a primary versus secondary drug effect could not be determined. In light of the histopathologic characteristics of the islet-centered changes seen with GDC-0853 involving compromised vascular integrity with resulting local acute hemorrhage and edema and chronic fibrosis, we attempted to image the rat pancreatic lesions using several modalities. By US, there were no significant differences between GDC-0853-treated and control animals in either b-mode or percent vascularity after 14 days. Furthermore, there were no differences in MRI or CT imaging parameters, the latter of which had shown promise in detecting fibrotic changes in patients experiencing pancreatic anastomotic failure following pancreatoduodenectomy (Hashimoto et al., 2011).

Despite the presence of significant pancreatic pathology, SD rats administered GDC-0853 demonstrated good overall tolerability with no related clinical signs. Additionally, no significant changes in standard clinical pathology parameters associated with exocrine or endocrine function were observed in studies up to 4 weeks in duration. There were no significant changes in serum amylase, lipase, insulin, or fructosamine

Downloaded from jpet.aspetjournals.org at ASPET Journals on April 18, 2024

JPET Fast Forward. Published on November 7, 2016 as DOI: 10.1124/jpet.116.236224
This article has not been copyedited and formatted. The final version may differ from this version.

(glycated serum albumin used to assess glycemic control over the preceding approximately 2 weeks). Fasted blood glucose was mildly increased in rats administered the highest dose of GDC-0853. However, given that pancreatic lesions of a similar incidence and severity were observed in animals at lower doses in this study with no apparent changes in glucose levels, the relationship between the minor increase in glucose levels and pancreatic lesions is uncertain. Elevated relative glucose levels were observed following OGTT at all doses of GDC-0853 where pancreatic lesions were observed, but these effects were detected only after 28 days (not after 4 or 14 days). Thus, there appear to be GDC-0853-related changes in glucose homeostasis, but the relationship to pancreatic findings has not been definitively established and may be considered either secondary to the development of the lesion or even a separate effect of BTK inhibitors in rats. Moreover, the relative timing and mild magnitude of the changes in glucose regulation in rats suggest that similar tests would be of questionable clinical utility for monitoring the onset of any pancreatic changes in a heterogeneous patient population.

In summary, our results suggest that BTK inhibitors, as a class, cause a pancreatic lesion in rats that may be due to exacerbation of a unique susceptibility of rats (especially in the SD strain) to develop peri-islet hemorrhage and subsequent inflammation and fibrosis. These pancreatic changes are subclinical, with few changes in standard clinical pathology parameters associated with exocrine or endocrine pancreatic function, suggesting significant functional reserve. These lesions were not detected by 3 imaging methods, making monitoring of development of the lesions difficult. Nonetheless, the absence of similar changes in other nonclinical species administered BTK inhibitors and in BTK

Downloaded from jpet.aspetjournals.org at ASPET Journals on April 18, 2024

JPET Fast Forward. Published on November 7, 2016 as DOI: 10.1124/jpet.116.236224
This article has not been copyedited and formatted. The final version may differ from this version.

mutant mouse models, and the lack of clinical reports of pancreatic dysfunction in patients with XLA and patients treated with ibrutinib argues that this type of injury is very unlikely to occur with BTK inhibitor therapeutics in humans.

Downloaded from jpet.aspetjournals.org at ASPET Journals on April 18, 2024

JPET Fast Forward. Published on November 7, 2016 as DOI: 10.1124/jpet.116.236224
This article has not been copyedited and formatted. The final version may differ from this version.

8. Acknowledgments

The authors thank Laura de Forge, Arna Katewa, Joseph Lubach, Michael Sweeney, and Covance Laboratories, Inc., for assistance in the conduct of the in vivo and ex vivo experiments.

Downloaded from jpet.aspetjournals.org at ASPET Journals on April 18, 2024

JPET Fast Forward. Published on November 7, 2016 as DOI: 10.1124/jpet.116.236224
This article has not been copyedited and formatted. The final version may differ from this version.

9. Authorship Contributions

Participated in research design: Erickson, Schutt, Tarrant, McDowell, Lewin-Koh, Hedehus, Ross, Carano, Staflin, Crawford, S. Zhong, Reif, Wong, Young, Dambach, Misner.

Conducted experiments: McDowell, Hedehus, Ross, Staflin, Katewa.

Contributed new reagents or analytic tools: McDowell, Hedehus, Ross, Carano, Crawford.

Performed data analysis: Erickson, Schutt, Tarrant, McDowell, Liu, Johnson, Lewin-Koh, Hedehus, Ross, Carano, Staflin, F. Zhong, Katewa, Wong, Misner.

Wrote or contributed to the writing of the manuscript: Erickson, Schutt, Tarrant, Johnson, Carano, Staflin, Wong, Young, Dambach, Misner.

Downloaded from jpet.aspetjournals.org at ASPET Journals on April 18, 2024

JPET Fast Forward. Published on November 7, 2016 as DOI: 10.1124/jpet.116.236224
This article has not been copyedited and formatted. The final version may differ from this version.

10. References

Aghamohammadi A, Fiorini M, Moin M, Parvaneh N, Teimourian S, Yeganeh M, Goffi F, Kanegane H, Amirzargar AA, Pourpak Z, Rezaei N, Salavati A, Pouladi N, Abdollahzade S, Notarangelo LD, Miyawaki T, and Plebani A (2006) Clinical, immunological and molecular characteristics of 37 Iranian patients with X-linked agammaglobulinemia. *Int Arch Allergy Immunol* **141:** 408–414.

Bao Y, Zheng J, Han C, Jin J, Han H, Liu Y, Lau Y-L, Tu W, and Cao X (2012) Tyrosine kinase Btk is required for NK cell activation. *J Biol Chem* **287**: 23769–23778.

Bonner-Weir S and O'Brien TD (2008) Islets in type 2 diabetes: in honor of Dr. Robert C. Turner. *Diabetes* **57**: 2899–2904.

Brenneman KA, Ramaiah SK, Rohde CM, Messing DM, O'Neil SP, Gauthier LM, Stewart ZS, Mantena SR, Shevlin KM, Leonard CG, Sokolowski SA, Lin H, Carraher DC, Jesson MI, Tomlinson L, Zhan Y, Bobrowski WF, Bailey SA, Vogel WM, Morris DL, Whiteley LO, and Davis JW 2nd (2014) Mechanistic investigations of test article-induced pancreatic toxicity at the endocrine-exocrine interface in the rat. *Toxicol Pathol* **42**: 229–242.

Brown JR, Harb WA, Hill BT, Gabrilove J, Sharman JP, Schreeder MT, Barr PM, Foran JM, Miller TP, Burger JA, Kelly KR, Mahadevan D, Ma S, Li Y, Pierce DW, Barnett E, Marine J, Miranda M, Azaryan A, Yu X, Nava-Parada P, Mei J, and Kipps TJ. (2016)

Downloaded from jpet.aspetjournals.org at ASPET Journals on April 18, 2024

JPET Fast Forward. Published on November 7, 2016 as DOI: 10.1124/jpet.116.236224
This article has not been copyedited and formatted. The final version may differ from this version.

Phase 1 study of single-agent CC-292, a highly selective Bruton's tyrosine kinase inhibitor, in relapsed or refractory chronic lymphocytic leukemia. *Haematologica*. **7**: 295-298.

Byrd JC, Harrington B, O'Brien S, Jones JA, Schuh A, Devereux S, Chaves J, Wierda, W.G., Awan, F.T., Brown, J.R, Hillmen P, Stephens DM, Ghia P, Barrientos JC, Pagel JM, Woyach J, Johnson D, Huang J, Wang X, Kaptein A, Lannutti BJ, Covey T, Fardis M, McGreivy J, Hamdy A, Rothbaum W, Izumi R, Diacovo TG, Johnson AJ, and Furman RR (2016) Acalabrutinib (ACP-196) in Relapsed Chronic Lymphocytic Leukemia. *N Engl J Med* **374**: 323–332.

Conley ME, Rohrer J, and Minegishi Y (2000) X-linked agammaglobulinemia. *Clin Rev Allergy Immunol* **19**: 183–204.

Dillberger JE (1994) Age-related pancreatic islet changes in Sprague-Dawley rats. *Toxicol Pathol* **22**: 48–55.

Donath MY, Schumann DM, Faulenbach M, Ellingsgaard H, Perren A, and Ehses JA (2008) Islet inflammation in type 2 diabetes: from metabolic stress to therapy. *Diabetes Care* **31**: S161–S164.

Downloaded from jpet.aspetjournals.org at ASPET Journals on April 18, 2024

JPET Fast Forward. Published on November 7, 2016 as DOI: 10.1124/jpet.116.236224
This article has not been copyedited and formatted. The final version may differ from this version.

Ellmeier W, Jung S, Sunshine MJ, Hatam F, Xu Y, Baltimore D, Mano H, and Littman DR (2000) Severe B cell deficiency in mice lacking the tec kinase family members Tec and Btk. *J Exp Med* **192**: 1611–1624.

Evans EK, Tester R, Aslanian S, Karp R, Sheets M, Labenski MT, Witowski SR, Lounsbury H, Chaturvedi P, Mazdiyasni H, Zhu Z, Nacht M, Freed MI, Petter RC, Dubrovskiy A, Singh J, and Westlin WF (2013) Inhibition of Btk with CC-292 provides early pharmacodynamic assessment of activity in mice and humans. *J Pharmacol Exp Ther* **346**: 219–228.

Goertz DE, Yu JL, Kerbel RS, Burns PN, and Foster FS (2002) High-frequency Doppler ultrasound monitors the effects of antivascular therapy on tumor blood flow. *Cancer Res* **62**: 6371–6375.

Greaves P (2012) Exocrine pancreas/endocrine pancreas, in *Histopathology of Preclinical Toxicity Studies: Interpretation and Relevance in Drug Safety Evaluation* pp 489–510, Academic Press, Amsterdam, Netherlands.

Hashimoto Y, Sclabas GM, Takahashi N, Kirihara Y, Smyrk TC, Huebner M, and Farnell MB (2011) Dual-phase computed tomography for assessment of pancreatic fibrosis and anastomotic failure risk following pancreatoduodenectomy. *J Gastrointest Surg Off J Soc Surg Aliment Tract* **15**: 2193–2204.

Downloaded from jpet.aspetjournals.org at ASPET Journals on April 18, 2024

JPET Fast Forward. Published on November 7, 2016 as DOI: 10.1124/jpet.116.236224
This article has not been copyedited and formatted. The final version may differ from this version.

Hayakawa K, Mimura Y, Tachibana S, Furuya M, Kodama T, Aoki T, Hosokawa S, Fukui M, Shibata S, Yoshida M, Masuyama T, Narita T, Kuwagata M, Hisada S, and Maki E (2013) Study for collecting background data on Wistar Hannover [Crl:WI(Han)] rats in general toxicity studies--comparative data to Sprague Dawley rats. *J Toxicol Sci* **38**: 855–873.

Herman SEM, Mustafa RZ, Gyamfi JA, Pittaluga S, Chang S, Chang B, Farooqui M, and Wiestner A (2014) Ibrutinib inhibits BCR and NF-κB signaling and reduces tumor proliferation in tissue-resident cells of patients with CLL. *Blood* **123**: 3286–3295.

Hermaszewski RA and Webster AD (1993) Primary hypogammaglobulinaemia: a survey of clinical manifestations and complications. *Q J Med* **86**: 31–42.

Howard V, Greene JM, Pahwa S, Winkelstein JA, Boyle JM, Kocak M, and Conley ME (2006) The health status and quality of life of adults with X-linked agammaglobulinemia. *Clin Immunol* **118**: 201–208.

Hull RL, Shen Z-P, Watts MR, Kodama K, Carr DB, Utzschneider KM, Zraika S, Wang F, and Kahn SE (2005) Long-term treatment with rosiglitazone and metformin reduces the extent of, but does not prevent, islet amyloid deposition in mice expressing the gene for human islet amyloid polypeptide. *Diabetes* **54**: 2235–2244.

Downloaded from jpet.aspetjournals.org at ASPET Journals on April 18, 2024

JPET Fast Forward. Published on November 7, 2016 as DOI: 10.1124/jpet.116.236224
This article has not been copyedited and formatted. The final version may differ from this version.

Iizuka S, Suzuki W, Tabuchi M, Nagata M, Imamura S, Kobayashi Y, Kanitani M, Yanagisawa T, Kase Y, Takeda S, Aburada M, Takahashi KW (2005) Diabetic complications in a new animal model (TSOD mouse) of spontaneous NIDDM with obesity. *Exp Anim* **54**: 71–83.

Imaoka M, Satoh H, and Furuhama K (2007) Age- and sex-related differences in spontaneous hemorrhage and fibrosis of the pancreatic islets in Sprague-Dawley rats. *Toxicol Pathol* **35**: 388–394.

Iyer AS, Morales JL, Huang W, Ojo F, Ning G, Wills E, Baines JD, and August A (2011) Absence of Tec family kinases interleukin-2 inducible T cell kinase (Itk) and Bruton's tyrosine kinase (Btk) severely impairs Fc epsilonRI-dependent mast cell responses. *J Biol Chem* **286**: 9503–9513.

Jones HB, Nugent D, and Jenkins R (2010) Variation in characteristics of islets of Langerhans in insulin-resistant, diabetic and non-diabetic-rat strains. *Int J Exp Pathol* **91**: 288–301.

Junger E, Herberg L, Jeruschke K, and Leiter EH (2002) The diabetes-prone NZO/Hl strain. II. Pancreatic immunopathology. *Lab Investig J Tech Methods Pathol* **82**: 843–853.

Downloaded from jpet.aspetjournals.org at ASPET Journals on April 18, 2024

JPET Fast Forward. Published on November 7, 2016 as DOI: 10.1124/jpet.116.236224
This article has not been copyedited and formatted. The final version may differ from this version.

Katsuda Y, Ohta T, Miyajima K, Kemmochi Y, Sasase T, Tong B, Shinohara M, and Yamada T (2014) Diabetic complications in obese type 2 diabetic rat models. *Exp Anim Jpn Assoc Lab Anim Sci* **63**: 121–132.

Kerner JD, Appleby MW, Mohr RN, Chien S, Rawlings DJ, Maliszewski CR, Witte ON, and Perlmutter RM (1995). Impaired expansion of mouse B cell progenitors lacking Btk. *Immunity* **3**: 301–312.

Lacraz G, Giroix M-H, Kassis N, Coulaud J, Galinier A, Noll C, Cornut M, Schmidlin F, Paul J-L, Janel N, Irminger JC, Kergoat M, Portha B, Donath MY, Ehses JA, and Homo-Delarche F. (2009) Islet endothelial activation and oxidative stress gene expression is reduced by IL-1Ra treatment in the type 2 diabetic GK rat. *PloS One* **4**: e6963.

Lederman HM, and Winkelstein JA (1985) X-linked agammaglobulinemia: an analysis of 96 patients. *Medicine (Baltimore)* **64**: 145–156.

Lindvall JM, Blomberg KEM, Väliaho J, Vargas L, Heinonen JE, Berglöf A, Mohamed AJ, Nore BF, Vihinen M, and Smith CIE (2005) Bruton's tyrosine kinase: cell biology, sequence conservation, mutation spectrum, siRNA modifications, and expression profiling. *Immunol Rev* **203**: 200–215.

Lipsky AH, Farooqui MZ, Tian X, Martyr S, Cullinane AM, Nghiem K, Sun C, Valdez J, Niemann CU, Herman SE, Saba N, Soto S, Marti G, Uzel G, Holland SM, Lozier JN, and

Downloaded from jpet.aspetjournals.org at ASPET Journals on April 18, 2024

JPET Fast Forward. Published on November 7, 2016 as DOI: 10.1124/jpet.116.236224
This article has not been copyedited and formatted. The final version may differ from this version.

Wiestner A (2015) Incidence and risk factors of bleeding-related adverse events in patients with chronic lymphocytic leukemia treated with ibrutinib. *Haematologica* **100**: 1571–1578.

McMullen JR, Boey EJH, Ooi JYY, Seymour JF, Keating MJ, and Tam CS (2014) Ibrutinib increases the risk of atrial fibrillation, potentially through inhibition of cardiac PI3K-Akt signaling. *Blood* **124**: 3829–3830.

Moin M, Aghamohammadi A, Farhoudi A, Pourpak Z, Rezaei N, Movahedi M, Gharagozlou M, Ghazi BMS, Zahed A, Abolmaali K, Mahmoudi M, Emami L, and Bashashati M (2004) X-linked agammaglobulinemia: a survey of 33 Iranian patients. *Immunol Invest* **33**: 81–93.

Molica S (2015) The clinical safety of ibrutinib in chronic lymphocytic leukemia. *Expert Opin Drug Saf* **14**: 1621–1629.

Ojiro K, Kitamura H, Shimada T, and Nakamura M (1993) A morphometrical study of the postnatal development of rat pancreatic islets, with special regard to the differences between Wistar and Sprague-Dawley strains. *Kaibogaku Zasshi* **68**: 190–203.

Pan Z, Scheerens H, Li SJ, Schultz BE, Sprengeler PA, Burrill LC, Mendonca RV, Sweeney MD, Scott KC, Grothaus PG, Jeffery DA, Spoerke JM, Honigberg LA, Young

Downloaded from jpet.aspetjournals.org at ASPET Journals on April 18, 2024

JPET Fast Forward. Published on November 7, 2016 as DOI: 10.1124/jpet.116.236224
This article has not been copyedited and formatted. The final version may differ from this version.

PR, Dalrymple SA, and Palmer JT (2007) Discovery of selective irreversible inhibitors for Bruton's tyrosine kinase. *ChemMedChem* **2**: 58–61.

Pharmacyclics, Inc. (2015). Imbruvica: Highlights of prescribing information. Retrieved from http://www.accessdata.fda.gov/drugsatfda_docs/label/2015/205552s002lbl.pdf

Plebani A, Soresina A, Rondelli R, Amato GM, Azzari C, Cardinale F, Cazzola G, Consolini R, De Mattia D, Dell'Erba G, Duse M, Fiorini M, Martino S, Martire B, Masi M, Monafo V, Moschese V, Notarangelo LD, Orlandi P, Panei P, Pession A, Pietrogrande MC, Pignata C, Quinti I, Ragno V, Rossi P, Sciotto A, and Stabile A; Italian Pediatric Group for XLA-AIEOP. (2002) Clinical, immunological, and molecular analysis in a large cohort of patients with X-linked agammaglobulinemia: an Italian multicenter study. *Clin Immunol* **104**: 221–230.

Rawlings DJ, Saffran DC, Tsukada S, Largaespada DA, Grimaldi JC, Cohen L, Mohr RN, Bazan JF, Howard M, and Copeland NG (1993) Mutation of unique region of Bruton's tyrosine kinase in immunodeficient XID mice. *Science* **261**: 358–361.

Reaven EP and Reaven GM (1981) Structure and function changes in the endocrine pancreas of aging rats with reference to the modulating effects of exercise and caloric restriction. *J Clin Invest* **68**: 75–84.

Downloaded from jpet.aspetjournals.org at ASPET Journals on April 18, 2024

JPET Fast Forward. Published on November 7, 2016 as DOI: 10.1124/jpet.116.236224
This article has not been copyedited and formatted. The final version may differ from this version.

Satterthwaite AB, Cheroutre H, Khan WN, Sideras P, and Witte ON (1997) Btk dosage determines sensitivity to B cell antigen receptor cross-linking. *Proc Natl Acad Sci U S A* **94**: 13152–13157.

Stephens DM and Spurgeon SE (2015) Ibrutinib in mantle cell lymphoma patients: glass half full? Evidence and opinion. *Ther Adv Hematol* **6**: 242–252.

Talchai C, Lin HV, Kitamura T, and Accili D (2009) Genetic and biochemical pathways of beta-cell failure in type 2 diabetes. *Diabetes Obes Metab* **11**: 38–45.

Winkelstein JA, Marino MC, Lederman HM, Jones SM, Sullivan K, Burks AW, Conley ME, Cunningham-Rundles C, and Ochs HD (2006) X-linked agammaglobulinemia: report on a United States registry of 201 patients. *Medicine (Baltimore)* **85**: 193–202.

Young W, and Crawford J. (2016). Discovery of GDC-0853: A Highly Potent, Selective and Non-Covalent BTK Inhibitor. American Chemistry Society; San Diego, CA.

Downloaded from jpet.aspetjournals.org at ASPET Journals on April 18, 2024

JPET Fast Forward. Published on November 7, 2016 as DOI: 10.1124/jpet.116.236224
This article has not been copyedited and formatted. The final version may differ from this version.

11. Footnotes

† This work was funded by Genentech, Inc.

* Corresponding author

Reprint requests sent to:

Leah K. Schutt

1 DNA Way, MS59

South San Francisco, CA, 94080

schutt.leah@gene.com

Downloaded from jpet.aspetjournals.org at ASPET Journals on April 18, 2024

JPET Fast Forward. Published on November 7, 2016 as DOI: 10.1124/jpet.116.236224
This article has not been copyedited and formatted. The final version may differ from this version.

12. Legends for Figures

Figure 1. Representative photomicrographs of pancreatic histopathology observed in Sprague Dawley rats following daily oral administration of GDC-0853 for 21 or 28 days are presented. **A**. Minimal peri-islet hemorrhage, Day 29. **B**. Islet/peri islet hemorrhage and fibrin with mixed cell infiltrates and exocrine degeneration/atrophy, Day 29. **C**. Islet/peri-islet fibroplasia/fibrosis with adjacent exocrine atrophy, Day 22. **D**. Multifocal lesions at different stages present concurrently, Day 29. **E**. Masson's trichrome stain highlighting collagen (blue) in peri-islet fibrosis, Day 22. **F**. Immunohistochemical labeling of smooth muscle actin, Day 22. **G**. Immunohistochemical labeling of CD 68, Day 22. **H**. Immunohistochemical labeling of cytokeratin 19, Day 22. A; bar = 50 μm. B, C, E, F, G, H; bar = 100 μm. D; bar = 500 μm.

Figure 2. Molecular structures of BTK inhibitors GDC-0853, GNE-309, ibrutinib, and spebrutinib.

Figure 3. Exposure to GDC-0853 in Sprague-Dawley rats relative to BTK (on-target) and off-target (BMX, FGR, SRC) kinase half-maximal inhibitory concentrations (IC_{50}) are presented. Pharmacokinetic profiles were plotted for the no-observed-adverse-effect level (NOAEL; 0.5 mg/kg/day) and low-observed-adverse-effect level (LOAEL; 5 mg/kg/day) doses identified in 28- and 7-day studies, respectively. Kinase IC_{50} values were determined in in vitro biochemical activity assays at Genentech (for BTK) or Invitrogen (for BMX, FGR, SRC) using ATP concentrations equal to the apparent Michaelis constant (Km) for each kinase.

Downloaded from jpet.aspetjournals.org at ASPET Journals on April 18, 2024

JPET Fast Forward. Published on November 7, 2016 as DOI: 10.1124/jpet.116.236224
This article has not been copyedited and formatted. The final version may differ from this version.

Figure 4. Strain sensitivity to BTK inhibitor-induced pancreatic lesions is presented. GDC-0853 (30 mg/kg/day) and GNE-309 (100 mg/kg/day) were administered orally for 14 consecutive days to Sprague-Dawley (SD), Fischer-344 (F-344), and Wistar-Han (WH) rats (n=6 males per group per strain). With each test article, pancreatic lesions were observed in 5, 1, and 0 SD, F-344, and WH rats, respectively. All lesions in SD rats were moderate in severity, whereas those in F-344 rats were minimal severity. Plasma concentrations (μM) of GDC-0853 and GNE-309 at 3 hours postdose are presented as mean ± standard deviation.

Figure 5. Relative Btk transcript expression (dCT) in pancreatic tissue from human and Sprague-Dawley rat is presented. Laser capture microscopy (LCM) was performed on exocrine and endocrine pancreas from rats. Transcriptional expression was analyzed by Fluidigm in human islets (4 samples), rat exocrine and islet tissues (3 samples each), and rat lymph nodes (3 samples). The results are normalized to 18S/baseline. Values are presented as mean ± standard deviation.

Figure 6. Amylase, lipase, insulin, and fructosamine levels in Sprague-Dawley rats (n≤15 per sex per group) following administration of GDC-0853 are presented. GDC-0853 was administered orally at doses of 0.5 to 100 mg/kg/day for 28 days. Values are presented as mean ± standard deviation.

Downloaded from jpet.aspetjournals.org at ASPET Journals on April 18, 2024

JPET Fast Forward. Published on November 7, 2016 as DOI: 10.1124/jpet.116.236224
This article has not been copyedited and formatted. The final version may differ from this version.

Figure 7. Glucose and insulin levels in Sprague-Dawley rats following administration of GDC-0853 are presented. GDC-0853 was administered orally at doses of 0.5 to 100 mg/kg/day for up to 32 days. Fasted serum glucose in rats (n≤15 per sex per group) was measured on Days 13 and 28 (panel on the left). An oral glucose tolerance test in rats (n=5 per sex per group) on Day 32 included blood glucose and serum insulin measurements (panels on the right). Values are presented as mean ± standard deviation. Significance was defined at $P < 0.05$. Vehicle is referred to as Veh in the figure.

Figure 8. Ultrasound imaging of the pancreas in Sprague-Dawley rats following administration of GNE-309 (n=8 males per group) or GDC-0853 (n=16 males per group) are presented. GNE-309 and GDC-0853 were administered orally at dose of 100 mg/kg/day and 30 mg/kg/day, respectively, for 14 days. B-mode intensity and percent vascularity were measured on Day 14. Values are presented as mean ± standard deviation. Significance was defined at $P < 0.05$. Vehicle is referred to as Veh in the figure.

Downloaded from jpet.aspetjournals.org at ASPET Journals on April 18, 2024

JPET Fast Forward. Published on November 7, 2016 as DOI: 10.1124/jpet.116.236224
This article has not been copyedited and formatted. The final version may differ from this version.

13. Tables

Table 1. In vivo study design.

Purpose	Duration (days)	Test article	Rat strain	Number (N) of animals	Dose levels (mg/kg)	Endpoints evaluated
Pilot toxicity	7	GDC-0853	SD	N=4/sex/group	0, 5, 15, 30	TKt, CP, PHP
General toxicity	28-32	GDC-0853	SD	N=15/sex/group, with N=5/sex/group undergoing a 28-day recovery period	0, 0.5, 10, 30, 100	TKs, CP, OGTT, PHP
Characterization of pancreas pathology	21	GDC-0853	SD	N=6 males/group	0, 0.5, 30	TKt, CP, PHP, IHC
Oral glucose metabolism	14	GDC-0853	SD	N=6 males/group	0, 10, 100	TKt, OGTT, PHP
Intravenous glucose metabolism	28	GDC-0853	SD	N=10 males/group	0, 30	TKt, IVGTT, PHP
Strain sensitivity	14	GDC-0853	SD, WH, F-344	N=6 males/group	0, 30	TKt, PHP
Strain sensitivity	14	GNE-309	SD, WH, F-344	N=6 males/group	0, 100	TKt, PHP
Doppler ultrasound imaging	14	GNE-309	SD	N=8 males/group	0, 100	TKt, US, PHP
Doppler ultrasound imaging	14	GDC-0853	SD	N=16 males/group	0, 30	TKt, US, PHP
Computed Tomography imaging	14	GDC-0853	SD	N=16 males/group	0, 30	TKt, CT, PHP
Magnetic Resonance imaging	14	GNE-309	SD	N=8 males/group	0, 100	TKt, MRI, PHP

Abbreviations: TKs, toxicokinetics in satellite animals; TKt, toxicokinetics in toxicity animals; CP, standard clinical pathology; PHP, standard pancreatic histopathology (hematoxylin and eosin); IHC, immunohistochemistry of pancreatic tissue.

Downloaded from jpet.aspetjournals.org at ASPET Journals on April 18, 2024

Table 2. Comparison of BTK inhibitors and results in Sprague-Dawley rats: BTK potency and selectivity, toxicokinetics, and incidence of pancreatic lesions

BTK inhibitor	Whole blood potency[1]		Kinases inhibited at 1 μM: > 50% or > 80% (**bolded**)[2]	Study Duration (days)	Dose (mg/kg/day)	C_{max}[3] (μM)	AUC_{0-24}[3] (hr · μM)	Incidence of pancreatic lesions[4]
	pBTK IC_{50} (nM)	CD69 IC_{50} (nM)						
GDC-0853	11 ± 4	8 ± 6	**BTK,** SRC, FGR, BMX	7	5	1.52	7.55	1/4 M, 0/4 F
					10	4.29	23.9	2/4 M, 0/4 F
					30	15.1	149	2/4 M, 0/4 F
GNE-309	15 ± 2	13 ± 3	**BTK,** SRC, FGR	7	30	4.17	17.4	0/4 M, 1/4 F
					100	17.7	183	2/4 M, 2/4 F
					300	54.8	566	2/4 M, 3/4 F
ibrutinib	7 ± 2	12 ± 1	**BTK, SRC, FGR, BMX, BLK, BRK, TEC, YES, RIPK2, HCK, CSK, LCK, LYN, TXK, ERBB4, ERBB2, EGFR, FRK, RET, SRM, TNK2, FLT3, ITK, JAK3,** FLT4, KDR, B-RAF, TIE2, CSF1R, FGF1R, PDGFRalpha	14	5	0.349	0.608	0/6 M, 1/6 F
					25	2.20	5.56	1/6 M, 1/6 F
spebrutinib	186 ± 214	392 ± 146	**BTK,** SRC, **BMX, STK16, TXK, TEC, JAK3**, ERBB4, ARK5, JNK1, RET, FLT3, AuroraA, JNK3, AuroraB, DRAK1, WEE1, JAK2, FLT4, IRAK1	14	30	1.00	2.66	3/6 M
					100	2.26	10.5	2/6 M
					300	6.64	36.3	1/6 M

Abbreviations: AUC_{0-24} = area under the concentration-time curve from time 0 to 24 hours; BTK = Bruton's tyrosine kinase; C_{max} = maximal concentration; F = female; IC_{50} = half-maximal inhibitory concentration; M = male.

[1] The mean IC_{50} ± standard deviation from 3 to 6 donors is presented.

[2] BTK inhibitors were tested against a panel of 221 active recombinant human kinases.

[3] Toxicokinetics performed on the last day of dosing: group mean C_{max} and AUC_{0-24} (male and female combined where relevant due to no appreciable sex differences).

[4] Not observed in any control animal treated with vehicle.

Downloaded from jpet.aspetjournals.org at ASPET Journals on April 18, 2024

JPET Fast Forward. Published on November 7, 2016 as DOI: 10.1124/jpet.116.236224
This article has not been copyedited and formatted. The final version may differ from this version.

JPET Fast Forward. Published on November 7, 2016 as DOI: 10.1124/jpet.116.236224
This article has not been copyedited and formatted. The final version may differ from this version.

Downloaded from jpet.aspetjournals.org at ASPET Journals on April 18, 2024

Figure 1

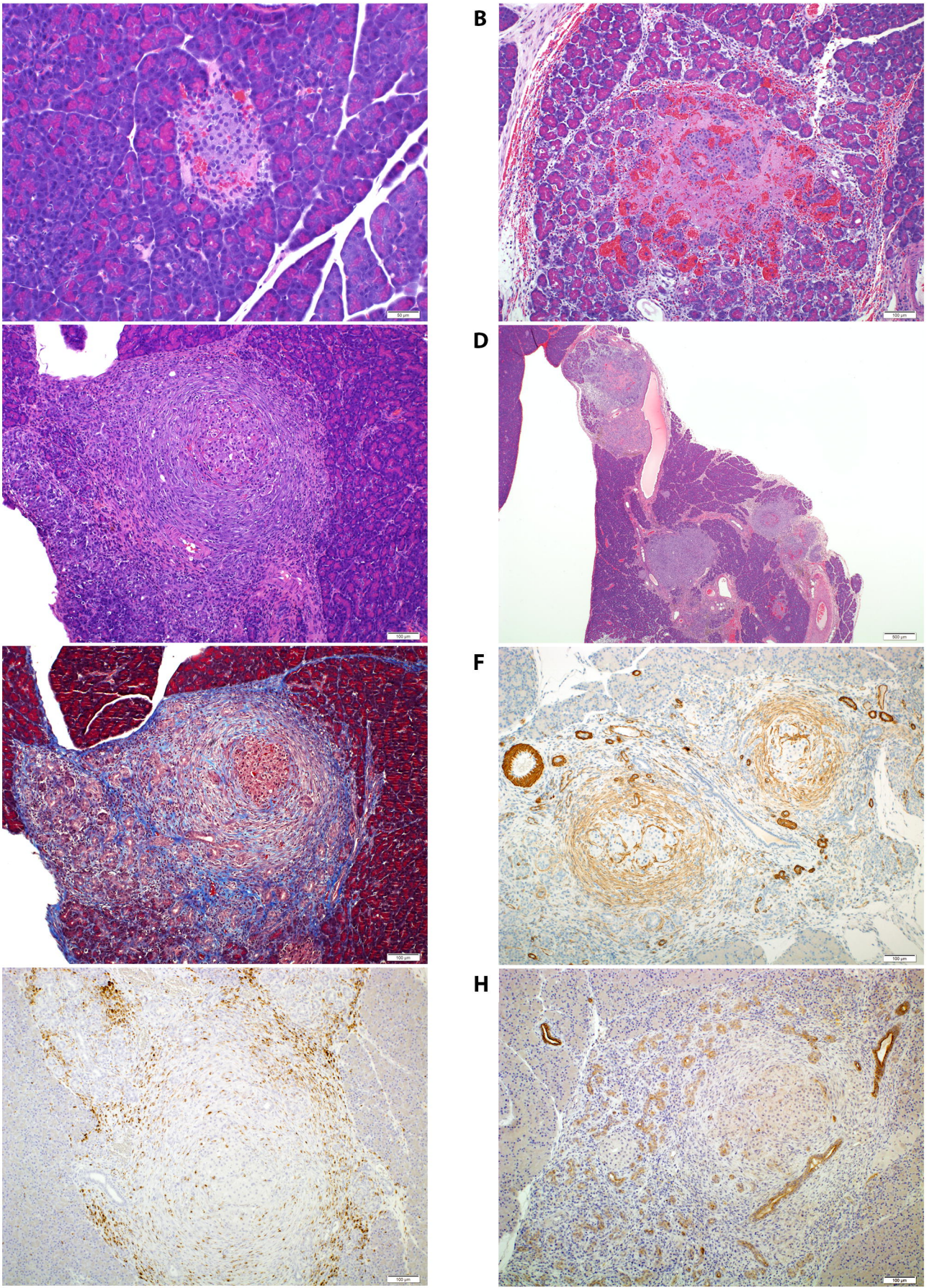

Figure 2

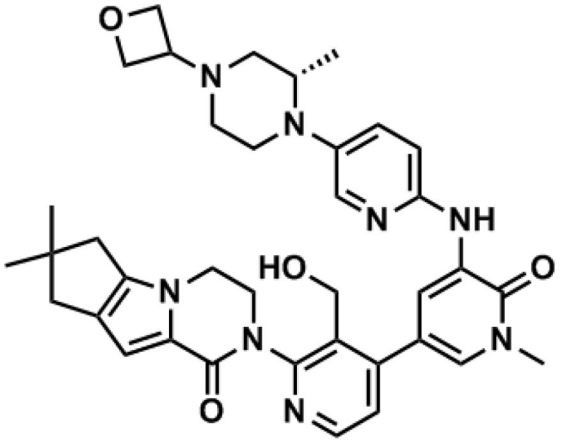

GDC-0853

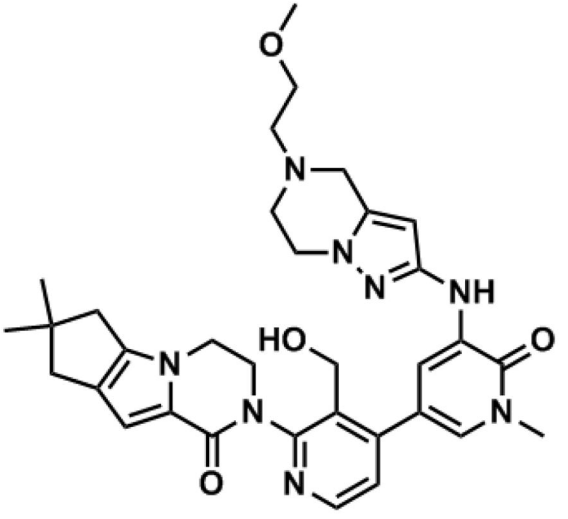

GNE-309

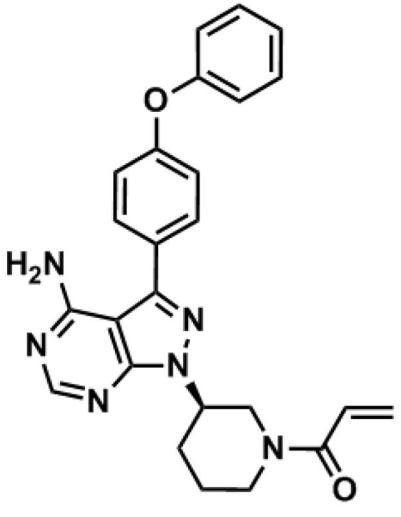

ibrutinib

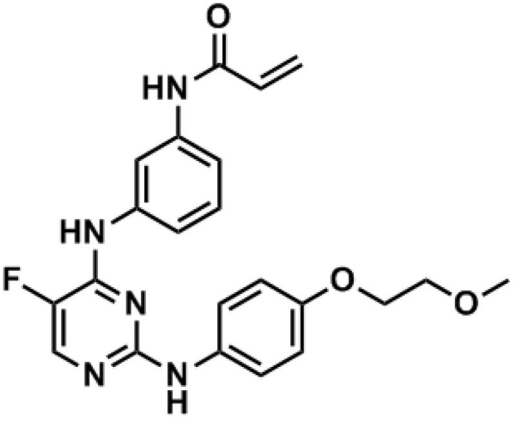

spebrutinib

Figure 3

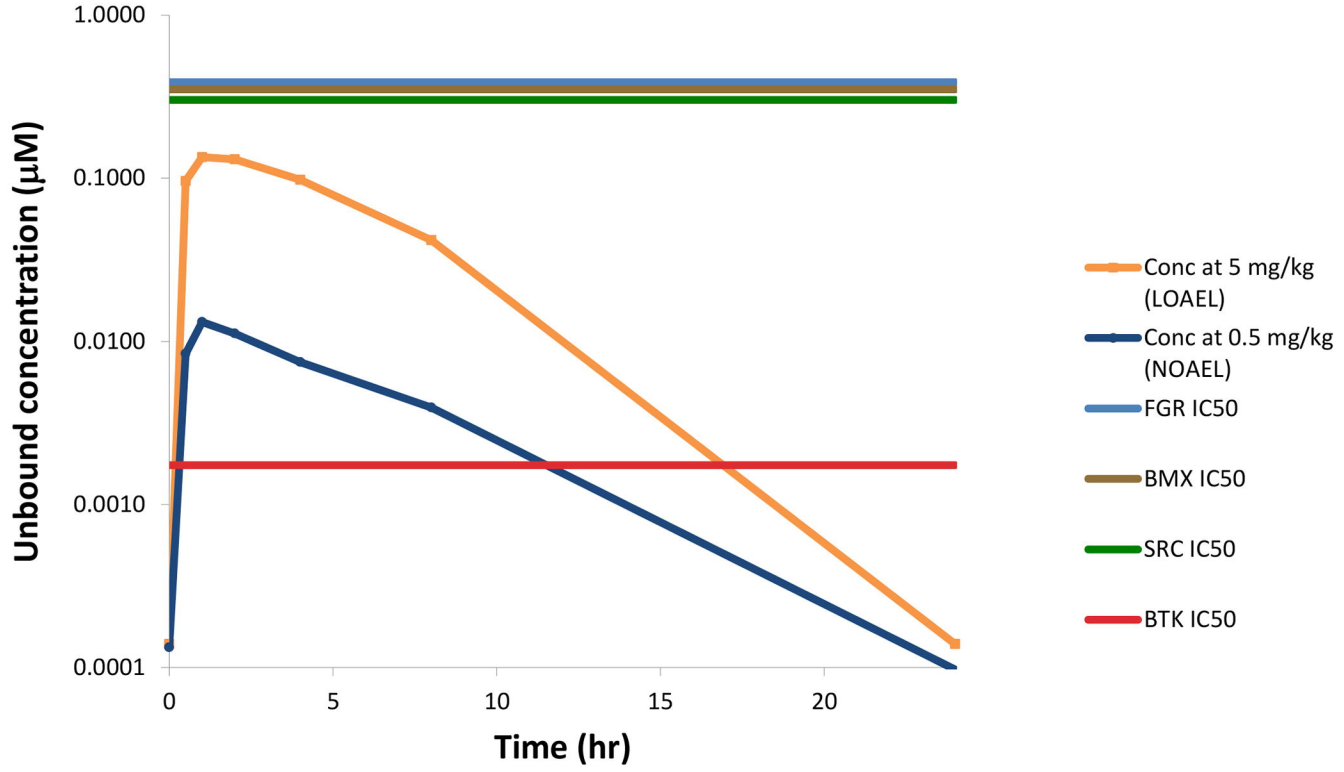
1.0000
0.1000
0.0100
0.0010
0.0001
Unbound concentration (µM)
0
5
10
15
20
Time (hr)
Conc at 5 mg/kg (LOAEL)
Conc at 0.5 mg/kg (NOAEL)
FGR IC50
BMX IC50
SRC IC50
BTK IC50

Figure 4

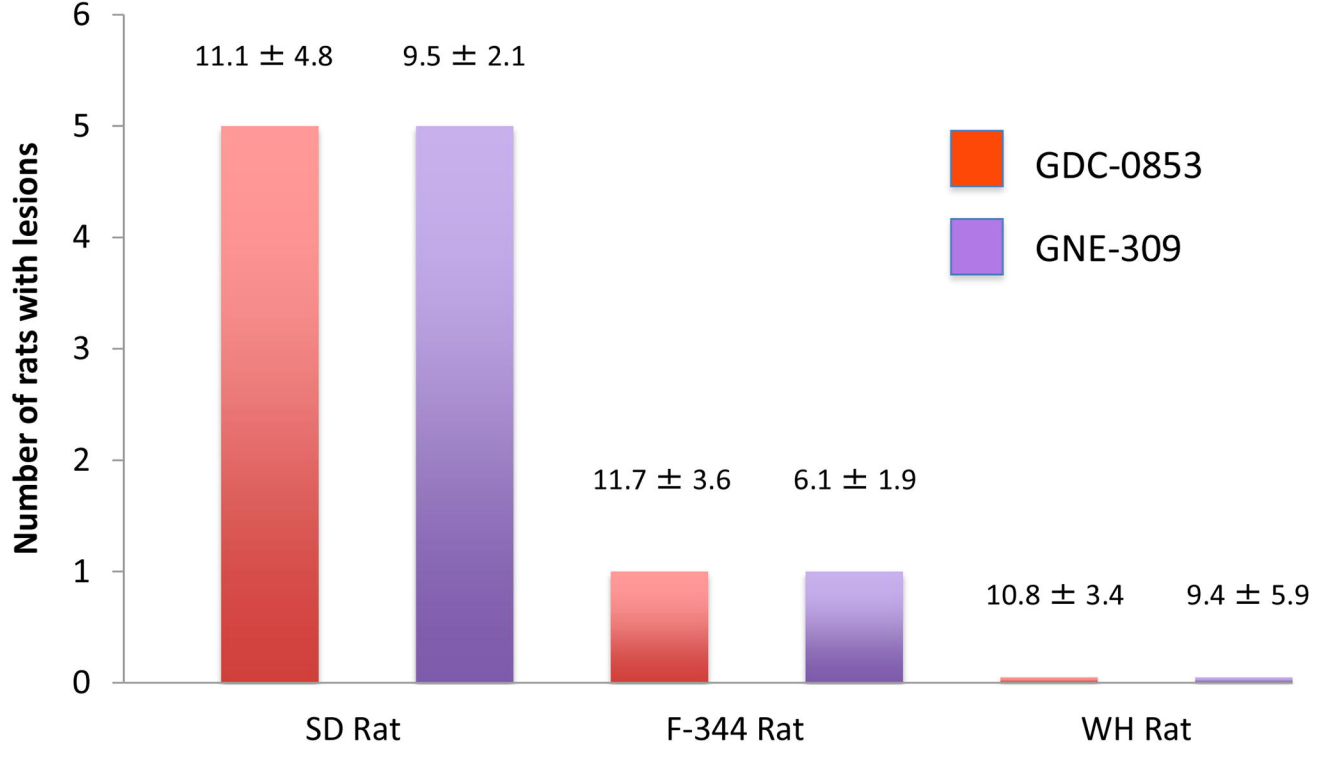
6
5
4
3
2
1
0
Number of rats with lesions
11.1 ± 4.8
9.5 ± 2.1
11.7 ± 3.6
6.1 ± 1.9
10.8 ± 3.4
9.4 ± 5.9
GDC-0853
GNE-309
SD Rat
F-344 Rat
WH Rat

Figure 5

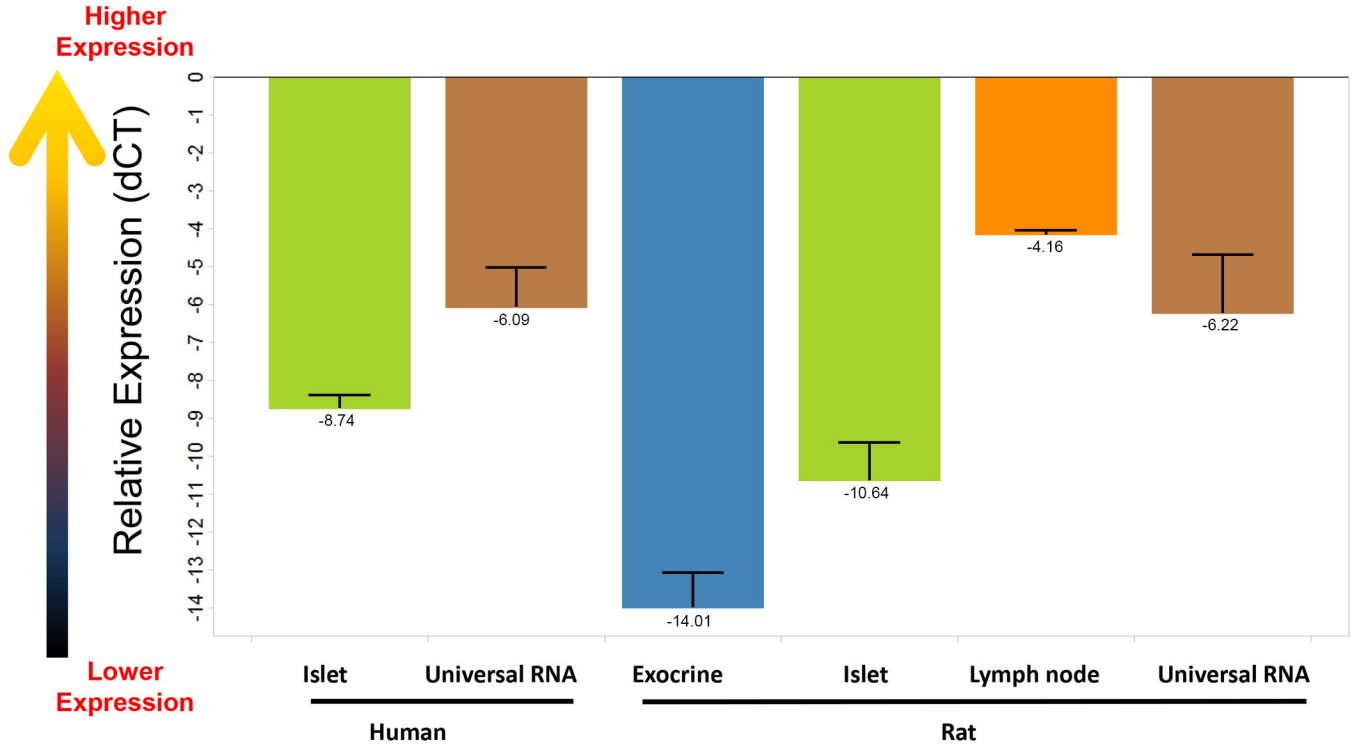
Higher Expression
Lower Expression
Relative Expression (dCT)
0
-1
-2
-3
-4
-5
-6
-7
-8
-9
-10
-11
-12
-13
-14
-8.74
-6.09
-14.01
-10.64
-4.16
-6.22
Islet
Universal RNA
Exocrine
Islet
Lymph node
Universal RNA
Human
Rat

Figure 6

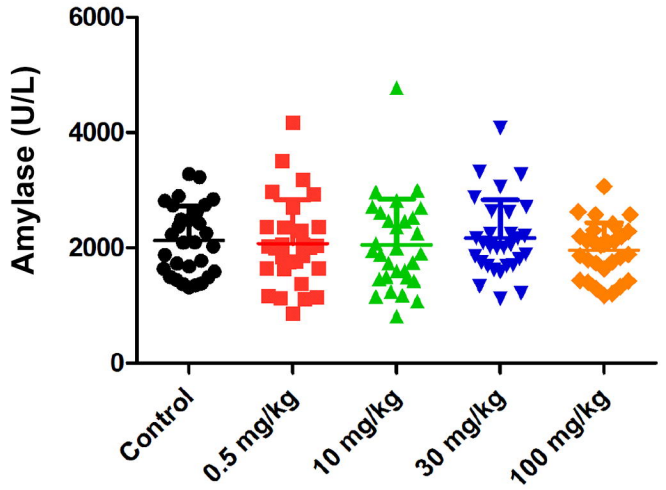
Amylase (U/L)
6000
4000
2000
0
Control
0.5 mg/kg
10 mg/kg
30 mg/kg
100 mg/kg

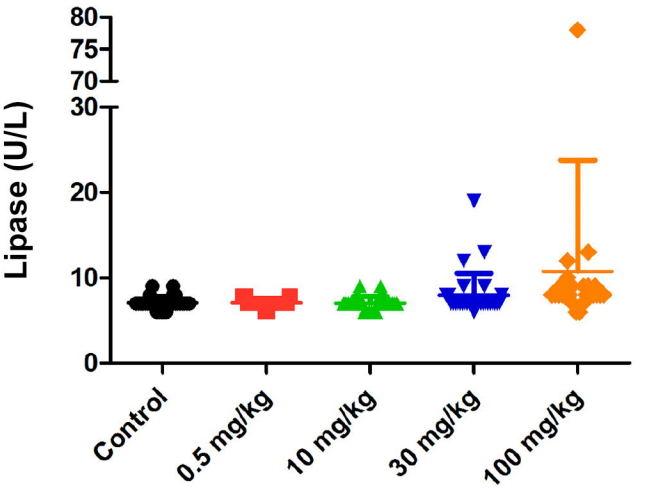
Lipase (U/L)
80
75
70
30
20
10
0
Control
0.5 mg/kg
10 mg/kg
30 mg/kg
100 mg/kg

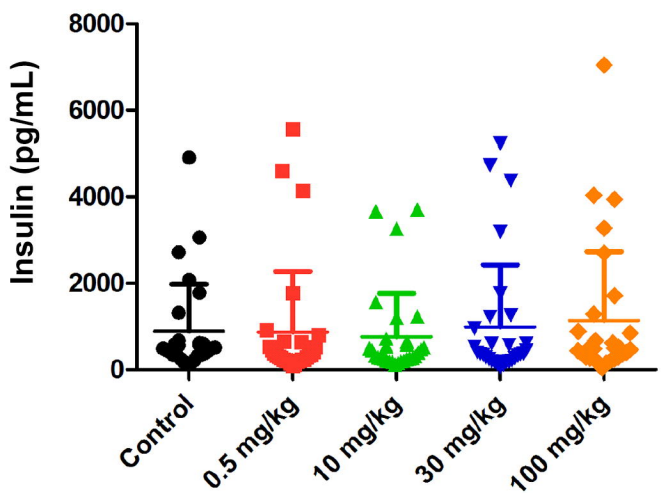
Insulin (pg/mL)
8000
6000
4000
2000
0
Control
0.5 mg/kg
10 mg/kg
30 mg/kg
100 mg/kg

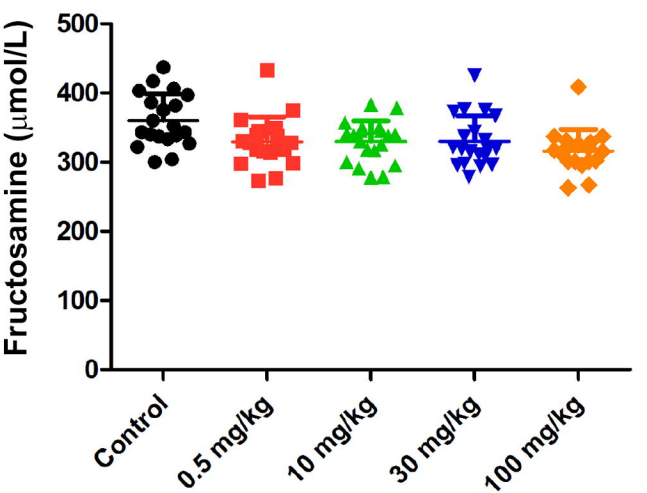
Fructosamine (μmol/L)
500
400
300
200
100
0
Control
0.5 mg/kg
10 mg/kg
30 mg/kg
100 mg/kg

Figure 7

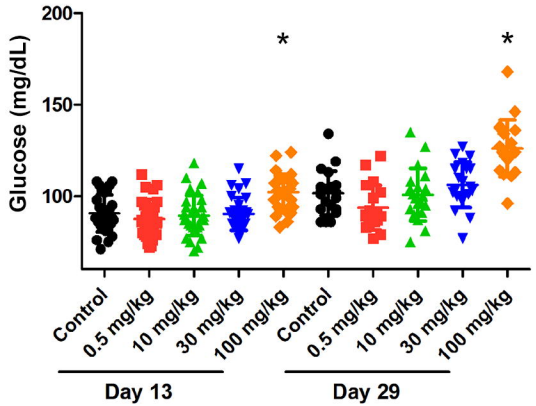
Glucose (mg/dL)
200
150
100
*
*
Control
0.5 mg/kg
10 mg/kg
30 mg/kg
100 mg/kg
Control
0.5 mg/kg
10 mg/kg
30 mg/kg
100 mg/kg
Day 13
Day 29

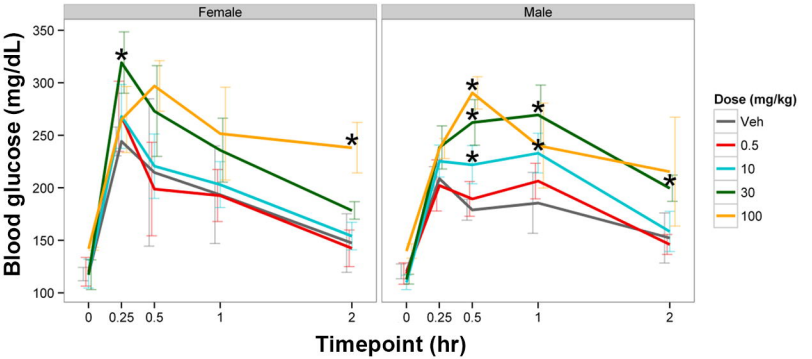
Female
Male
Blood glucose (mg/dL)
350
300
250
200
150
100
0
0.25
0.5
1
2
Timepoint (hr)
Dose (mg/kg)
Veh
0.5
10
30
100

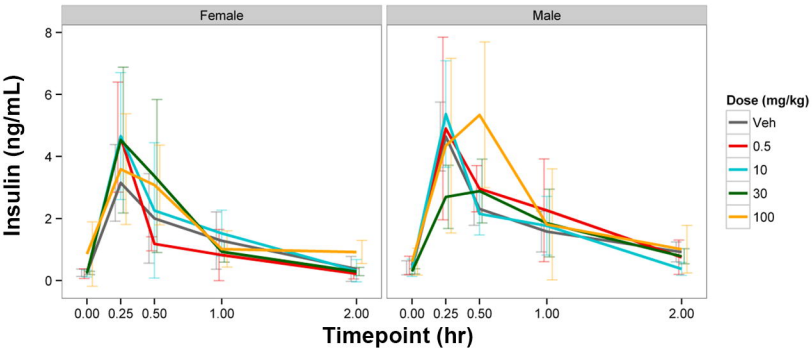
Female
Male
Insulin (ng/mL)
8
6
4
2
0
0.00
0.25
0.50
1.00
2.00
Timepoint (hr)
Dose (mg/kg)
Veh
0.5
10
30
100

Figure 8

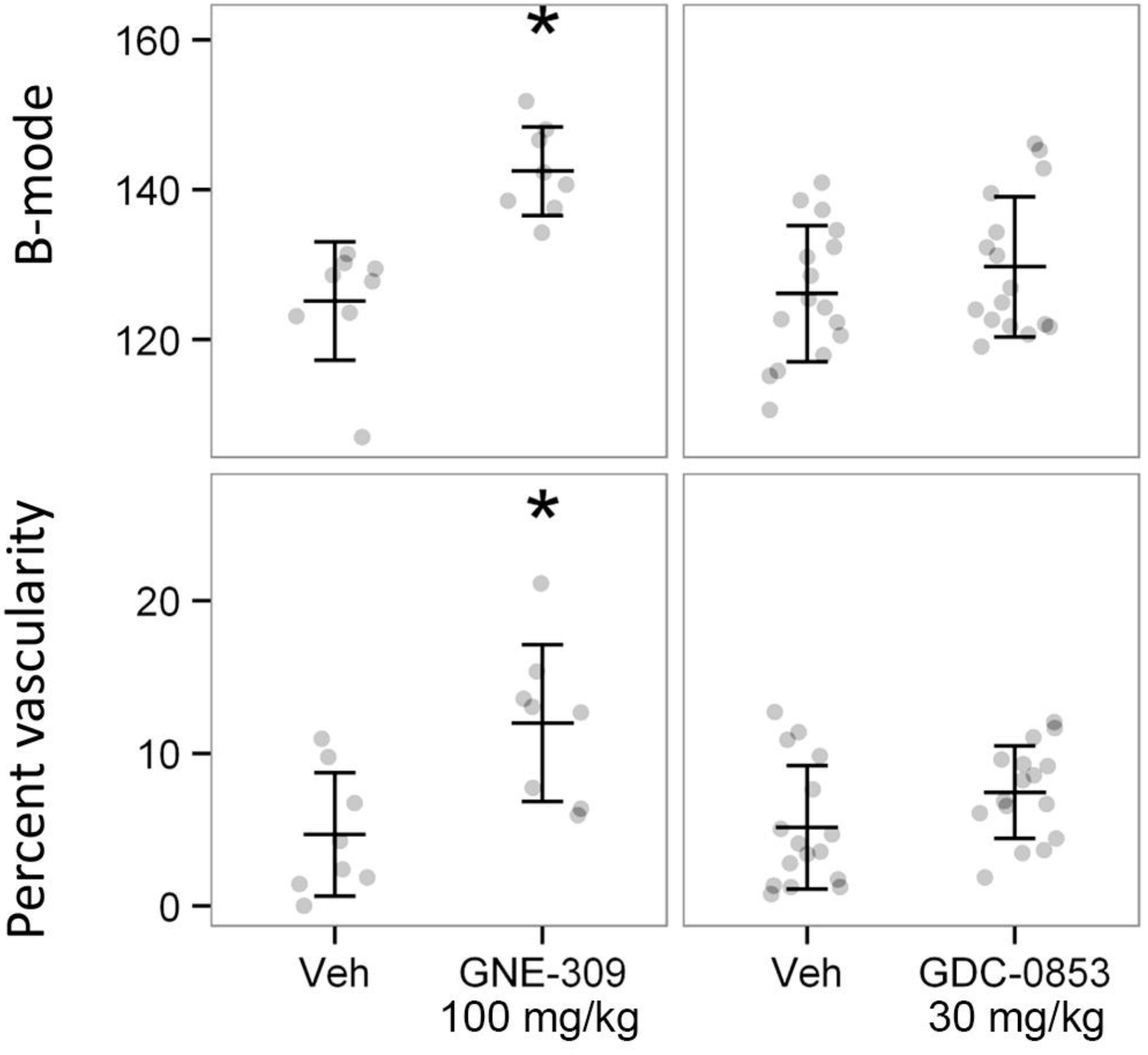
B-mode
160
140
120
*
Percent vascularity
20
10
0
*
Veh
GNE-309
100 mg/kg
Veh
GDC-0853
30 mg/kg